SIAM J. NUMER. ANAL.
Vol. 50, No. 3, pp. 1801–1826

ANALYSIS OF AN *hp*-NONCONFORMING DISCONTINUOUS GALERKIN SPECTRAL ELEMENT METHOD FOR WAVE PROPAGATION*

TAN BUI-THANH† AND OMAR GHATTAS‡

Abstract. We analyze the consistency, stability, and convergence of an *hp* discontinuous Galerkin spectral element method of Kopriva [*J. Comput. Phys.*, 128 (1996), pp. 475–488] and Kopriva, Woodruff, and Hussaini [*Internat. J. Numer. Methods Engrg.*, 53 (2002), pp. 105–122]. The analysis is carried out simultaneously for acoustic, elastic, coupled elastic-acoustic, and electromagnetic wave propagation. Our analytical results are developed for both conforming and nonconforming approximations on hexahedral meshes using either exact integration with Legendre–Gauss quadrature or inexact integration with Legendre–Gauss–Lobatto quadrature. A mortar-based nonconforming approximation is developed to treat both *h*- and *p*-nonconforming meshes simultaneously. The mortar approach is constructed in such a way that consistency, stability, and convergence analyses for nonconforming approximations follow the conforming counterparts with minimal modifications. In particular, it casts *hp*-nonconforming interfaces into equivalent conforming faces on mortars, for which the analyses are easily carried out using standard approaches. Sharp *hp*-convergence results are then proved for nonconforming approximations of time-dependent wave propagation problems using both exact and inexact quadratures.

Key words. discontinuous Galerkin method, spectral element method, linear hyperbolic equations, acoustic, elastic, and electromagnetic wave propagation, Riemann flux, nonconforming meshes, Legendre–Gauss, Legendre–Gauss–Lobatto, consistency, stability, convergence

AMS subject classifications. 65N35, 65N12, 65N15

DOI. 10.1137/110828010

1. Introduction.

The discontinuous Galerkin (DG) method was originally developed by Reed and Hill [23] for the neutron transport equation, but it has been extended to other problems governed by partial differential equations (PDEs) [10]. In particular, it has emerged as a particularly attractive method for hyperbolic PDEs [9, 11]. Roughly speaking, DG combines advantages of classical finite volume and finite element methods. In particular, it has the ability to treat solutions with large gradients including shocks, it provides the flexibility to deal with complex geometries, and it is highly parallelizable due to its compact stencil. Perhaps its most important advantage, however, is its ability to support *hp* adaptivity (where *h* refers to mesh size, and *p* to local polynomial order) in a natural manner [5]. Together, these advantages make DG a very desirable method for parallel solution of large-scale hyperbolic problems on adapted meshes (e.g., [29]).

The question of how to treat nonconforming interfaces between elements due to both local *p*-refinement and local *h*-refinement can be addressed in several ways. The *hp*-nonconforming approach of Kopriva [16, 20] replaces nonconforming faces by mortars that connect pairs of contributing elements. (See [6] and [16] and the references

*Received by the editors March 21, 2011; accepted for publication (in revised form) February 17, 2012; published electronically June 28, 2012. This work was supported by AFOSR grant FA9550-09-1-0608 and NSF grants CDI-1028889 and DMS-0724746.

http://www.siam.org/journals/sinum/50-3/82801.html

†Institute for Computational Engineering & Sciences, The University of Texas at Austin, Austin, TX 78712 (buithanhtan2000@yahoo.com).

‡Institute for Computational Engineering & Sciences, Jackson School of Geosciences, and Department of Mechanical Engineering, The University of Texas at Austin, Austin, TX 78712 (omar@ices.utexas.edu).

therein for the differences between mortar methods for elliptic PDEs and those for hyperbolic PDEs.) The actual computations are performed on the mortars instead of the nonconforming faces, and the results are then projected onto the contributing element faces. Since the mortar approach maintains the compact stencil of the DG method, it makes adaptivity highly parallelizable [29]. Moreover, discrete stability and optimal convergence rates have been numerically observed in practice [20, 29]. Since then, there have been no attempts to theoretically study the stability and convergence of Kopriva's mortar-based *hp*-nonconforming approximation in the context of discontinuous Galerkin spectral element methods [15]. This is the subject of the present article in which we give the first attempt in providing a rigorous theoretical foundation for the method.

The celebrated Lax–Richtmyer equivalence theorem [22] has far-reaching consequences in numerical analysis, so much so that it is sometimes called the fundamental theorem of numerical analysis. The theorem says that for well-posed linear differential problems, consistency and stability of a difference method imply its convergence. However, typical applications of the Lax–Richtmyer theorem provide an upper bound on the error that grows exponentially in time. In practice, it is observed that the error grows at a much lower rate. Rather than rely on the equivalence theorem, it has been shown that a direct proof of convergence, with an error bound that grows at most linearly in time, is possible for a class of DG methods [13, 14].

In this paper, we study theoretically the consistency, stability, and convergence of an *hp*-nonconforming discontinuous Galerkin spectral element method (DGSEM) of Kopriva (see [16, 20, 29]) using such a direct proof. In particular, we present a stability proof using an energy method for the DGSEM with the mortar-based nonconforming approximation of Kopriva [16] and Kopriva, Woodruff, and Hussaini [20]. We expect that the results of our study can be applied to a large class of linear conservation laws. However, for concreteness, the proof is simultaneously carried out for elastic, acoustic, coupled elastic-acoustic, and electromagnetic wave equations, as exemplary conservation laws governed by linear hyperbolic PDEs. Instead of using an exact numerical quadrature for least-squares projections on mortars as in [20, 29], for which we are not able to prove stability in the interesting case of Legendre–Gauss–Lobatto quadrature, we propose to employ an adaptive quadrature rule that not only facilitates the stability proof but is also cheaper. At the heart of our strategy is the ability to cast computations on nonconforming faces into equivalent conforming computations on mortars, for which the analysis is easier to carry out.

We are able to prove stability and convergence for both exact numerical quadrature using the Legendre–Gauss rule and inexact numerical quadrature using the Legendre–Gauss–Lobatto rule. For the inexact numerical integration, we use the tensor product quadrature rule, since it allows us to perform discrete integration by parts [26, 19], which in turns paves the way for the stability and convergence proofs.

The Riemann numerical flux is our main ingredient in proving stability and convergence. Since the PDEs in this paper are linear, the exact Riemann flux can be derived [27], and therefore we use it in our proofs. As will be shown, it is the dissipative nature of the Riemann flux that makes the DGSEM stable. Therefore, we speculate that our results also hold for other dissipative fluxes such as the stabilized Lax–Friedrichs numerical flux [24].

We mostly restrict ourselves to the case of affine hexahedral meshes, for which details of the derivations and proofs are presented. In order to make the proofs concrete, three-dimensional coupled elastic-acoustic and electromagnetic waves are used as examples. Of course, all of the results hold for two-dimensional problems as well.

This article is organized as follows. Section 2 briefly describes a weak setting for general linear conservation laws. Section 3 presents an *hp* DGSEM for both elastic-acoustic and electromagnetic waves. We then prove stability for conforming meshes in section 4. The detailed description of our mortar-based nonconforming approximation is given in section 5, which is followed by the nonconforming stability proof in section 6. The direct proof of convergence is carried out in section 7, and section 8 offers conclusions.

2. General setting for linear hyperbolic conservation laws. We are interested in linear wave equations governed by linear hyperbolic conservation laws. In the strong form, a general equation is given as

$$\mathcal{Q}\frac{\partial \mathfrak{q}}{\partial t} + \nabla_{\boldsymbol{x}} \cdot (\mathfrak{F}\mathfrak{q}) = \mathfrak{g}, \quad \mathfrak{q} \in \mathcal{V},\ \boldsymbol{x} \in \mathcal{D},$$

with $\mathcal{V}$ as the solution space, to be specified later, over the domain of interest $\mathcal{D}$, and with appropriate initial and boundary conditions. The subscript $\boldsymbol{x}$ denotes the $\boldsymbol{x}$-coordinate system in which the divergence operator acts. Next, multiplying by the test function $\mathfrak{p}$, the corresponding weak formulation is obtained as

$$\int_{\mathcal{D}} \mathcal{Q}\frac{\partial \mathfrak{q}}{\partial t} \cdot \mathfrak{p}\, d\boldsymbol{x} + \int_{\mathcal{D}} \nabla_{\boldsymbol{x}} \cdot (\mathfrak{F}\mathfrak{q}) \cdot \mathfrak{p}\, d\boldsymbol{x} = \int_{\mathcal{D}} \mathfrak{g} \cdot \mathfrak{p}\, d\boldsymbol{x},$$

where "$\cdot$" denotes the Euclidean inner product.

We next partition the domain $\mathcal{D}$ into n_{el} nonoverlapping hexahedral elements such that $\mathcal{D} = \bigcup_{e=1}^{n_{\mathrm{el}}} \mathsf{D}^e$ and integrate the weak formulation by parts twice to obtain

$$\begin{aligned} &\sum_e \int_{\mathsf{D}^e} \mathcal{Q}^e \frac{\partial \mathfrak{q}^e}{\partial t} \cdot \mathfrak{p}^e\, d\boldsymbol{x} + \int_{\mathsf{D}^e} \nabla_{\boldsymbol{x}} \cdot (\mathfrak{F}\mathfrak{q}^e) \cdot \mathfrak{p}^e\, d\boldsymbol{x} \\ &\quad + \int_{\partial \mathsf{D}^e} \boldsymbol{n} \cdot \left[(\mathfrak{F}\mathfrak{q}^e)^* - \mathfrak{F}\mathfrak{q}^e \right] \cdot \mathfrak{p}^e\, d\boldsymbol{s} = \sum_e \int_{\mathsf{D}^e} \mathfrak{g}^e \cdot \mathfrak{p}^e\, d\boldsymbol{x}, \end{aligned} \tag{2.1}$$

where a consistent numerical flux $(\mathfrak{F}\mathfrak{q}^e)^*$ has been introduced to couple solutions of neighboring elements, and $(\cdot)^e$ denotes the restriction on the eth element of the corresponding quantity.

Equation (2.1) is known as the strong form in the context of nodal DG methods [14]. For the DGSEM described in this paper, the strong form (integrating the flux terms by parts twice) and the weak form (integrating the flux terms by parts once) are equivalent [26, 19], and hence all the results in the paper hold for the weak form as well.

3. A discontinuous Galerkin spectral element method. In this section, we briefly describe an *hp*-DSEM. We assume that each element D^e is mapped to the reference hexahedron $\hat{\mathsf{D}} = [-1, 1]^3$ by a C^1-diffeomorphism $\boldsymbol{X}^e$ and that $\mathcal{D} \approx \mathcal{D}^{N_{el}} = \bigcup_{e=1}^{N_{el}} \mathsf{D}^e$. Equation (2.1) can be written in terms of $\hat{\mathsf{D}}$ as

$$\begin{aligned} &\sum_e \int_{\hat{\mathsf{D}}} J^e \mathcal{Q}^e \frac{\partial \mathfrak{q}^e}{\partial t} \cdot \mathfrak{p}^e\, d\boldsymbol{r} + \int_{\hat{\mathsf{D}}} \nabla_{\boldsymbol{r}} \cdot \left(\tilde{\mathfrak{F}}\mathfrak{q}^e \right) \cdot \mathfrak{p}^e\, d\boldsymbol{r} \\ &\quad + \int_{\partial \hat{\mathsf{D}}} \tilde{\boldsymbol{n}} \cdot \left[\left(\tilde{\mathfrak{F}}\mathfrak{q}^e \right)^* - \tilde{\mathfrak{F}}\mathfrak{q}^e \right] \cdot \mathfrak{p}^e\, d\boldsymbol{s} = \sum_e \int_{\hat{\mathsf{D}}} J^e \mathfrak{g}^e \cdot \mathfrak{p}^e\, d\boldsymbol{r}, \end{aligned} \tag{3.1}$$

where $\boldsymbol{r} = (r_1, r_2, r_3) \in \hat{\mathsf{D}}$ represents the reference coordinates and J^e is the Jacobian of the transformation. The outward normal on the boundary of the master element $\hat{\mathsf{D}}$ is denoted by $\tilde{\boldsymbol{n}}$, and the contravariant flux [17] is defined as

$$\tilde{\mathfrak{F}}^i = J^e \boldsymbol{a}^i \cdot \mathfrak{F}, \quad i = 1, 2, 3,$$

with $\boldsymbol{a}^i$ as the contravariant basis vectors.

We now describe the approximation spaces for wave propagation in elastic, acoustic, and coupled elastic-acoustic media using the strain-velocity formulation, and for Maxwell's equations for electromagnetic wave propagation. Equation (3.1) can be specialized to the elastic-acoustic wave propagation case by the definitions

$$\mathfrak{q} = \begin{pmatrix} \boldsymbol{E} \\ \boldsymbol{v} \end{pmatrix} \in \mathcal{V}, \quad \mathcal{Q} = \begin{pmatrix} \mathsf{I} & \mathbf{0} \\ \mathbf{0} & \rho \boldsymbol{I} \end{pmatrix}, \quad \mathfrak{g} = \begin{pmatrix} \mathbf{0} \\ \boldsymbol{f} \end{pmatrix} \in \mathcal{V},$$

with I denoting the fourth-order identity tensor, $\mathbf{0}$ the zero tensors of appropriate sizes, $\boldsymbol{I}$ the second-order identity tensor, $\boldsymbol{E}$ the strain tensor, $\boldsymbol{v}$ the velocity vector, $\boldsymbol{f}$ the external volumetric forces, and ρ the density. In order to justify the above notation, we note that the strain tensor $\boldsymbol{E}$ with values in $\mathbb{R}^{3\times 3}$ can be identified with a vector-valued field $\overline{\boldsymbol{E}}$ in $\mathbb{R}^9$ (since finite dimensional spaces with the same dimension are isomorphic) by setting $\overline{\boldsymbol{E}}_{[ij]} = \boldsymbol{E}_{ij}$ with $[ij] = 3(j-1)+i$. However, to simplify the notation we use the same symbol $\boldsymbol{E}$ for both tensor-valued and vector-valued fields, and this should be clear in each context. Similar identifications for other tensors are straightforward. These rigorous identifications make our exposition succinct to leave space for the analysis, which is the main focus of the paper.

The action of the flux operator $\mathfrak{F}$ on the strain-velocity unknowns $\mathfrak{q}$ can be shown to be [29]

$$(\mathfrak{F}\mathfrak{q})_i = \begin{pmatrix} -\frac{1}{2}\left(\boldsymbol{v} \otimes \boldsymbol{e}_i + \boldsymbol{e}_i \otimes \boldsymbol{v}\right) \\ -\left(\mathsf{C}\boldsymbol{E}\right)\boldsymbol{e}_i \end{pmatrix} \in \mathcal{V} \quad \text{for } i = 1, 2, 3,$$

where $\boldsymbol{e}_i$'s are the canonical basis vectors in $\mathbb{R}^3$ and the second-order tensor $\boldsymbol{v} \otimes \boldsymbol{e}_i$ is the standard dyadic product of vectors $\boldsymbol{v}$ and $\boldsymbol{e}_i$. For isotropic linear elasticity, the strain tensor $\boldsymbol{E}$ and the Cauchy stress tensor $\boldsymbol{S}$ are related by the fourth-order constitutive tensor C:

$$\boldsymbol{S} = \mathsf{C}\boldsymbol{E} = \lambda \operatorname{tr}(\boldsymbol{E})\boldsymbol{I} + 2\mu\boldsymbol{E},$$

where λ and μ are the two Lamé constants characterizing the isotropic constitutive relationship. The longitudinal wave speed c_p and shear wave speed c_s are defined in terms of the Lamé constants and density by

$$c_p = \sqrt{\frac{\lambda + 2\mu}{\rho}} \qquad \text{and} \qquad c_s = \sqrt{\frac{\mu}{\rho}},$$

with $c_s = 0$ in acoustic regions by virtue of $\mu = 0$.

As in [29], we choose the solution space to be $\mathcal{V} = \boldsymbol{V}_{\text{sym}}^{3\times 3} \oplus \boldsymbol{V}^3$, where $\boldsymbol{V}$ denotes a space of sufficiently smooth functions defined on $\mathcal{D}$ so that (2.1) makes sense (see Theorem 4 for examples of $\boldsymbol{V}$), and $\boldsymbol{V}_{\text{sym}}^{3\times 3}$ denotes the space of 3×3 symmetric matrices with elements in $\boldsymbol{V}$. The discontinuous approximation to $\boldsymbol{V}$ is given by

$$\boldsymbol{V}_d := \{q_d \in L^2(\mathcal{D}^{n_{\text{el}}}) : q_d|_{\mathsf{D}^e} \circ \boldsymbol{X}^e \in \mathbb{Q}_{N_e}(\hat{\mathsf{D}})\},$$

where $\mathbb{Q}_{N_e}$ is the tensor product of one-dimensional polynomials of degree at most N_e on the reference element. It should be pointed out that the polynomial orders need not be the same for all directions. Nevertheless, we use the same order for clarity of the exposition. The numerical solution $\mathfrak{q}_d \in \mathcal{V}_d = \boldsymbol{V}_{d,\mathrm{sym}}^{3\times 3} \oplus \boldsymbol{V}_d^3$ restricted on each element D^e is specified as

$$\mathfrak{q}_d|_{\mathsf{D}^e} \circ \boldsymbol{X}^e \in \mathcal{V}_d^e \equiv \mathbb{Q}_{N_e,\mathrm{sym}}^{3\times 3} \oplus \mathbb{Q}_{N_e}^3, \qquad \boldsymbol{X}^e : \hat{\mathsf{D}} \to \mathsf{D}^e,$$

Before introducing the Riemann flux, let us recall the following standard DG notation for quantities associated with element interfaces:

$$[\![\mathfrak{q}]\!] = \mathfrak{q}^+ \cdot \boldsymbol{n}^+ + \mathfrak{q}^- \cdot \boldsymbol{n}^-, \quad [\mathfrak{q}] = \mathfrak{q}^- - \mathfrak{q}^+, \quad \{\{Z\}\} = \frac{Z^+ + Z^-}{2},$$

where the positive and negative signs indicate element interior and exterior, respectively.

For linear conservation laws one can solve the Riemann problem exactly by various methods [27]. Using the Rankine–Hugoniot approach, Wilcox et al. [29] show that the exact Riemann flux for the strain equation is given by

$$\begin{aligned}\boldsymbol{n} \cdot \left[(\mathfrak{F}\mathfrak{q})_{\boldsymbol{E}}^* - (\mathfrak{F}\mathfrak{q})_{\boldsymbol{E}}\right] = {} & \left(k_0 \boldsymbol{n} \cdot [\![\mathsf{C}\boldsymbol{E}]\!] + k_0 \rho^+ c_p^+ [\![\boldsymbol{v}]\!]\right) \boldsymbol{n} \otimes \boldsymbol{n} \\ & - k_1 \operatorname{sym}\left(\boldsymbol{n} \otimes (\boldsymbol{n} \times (\boldsymbol{n} \times [\![\mathsf{C}\boldsymbol{E}]\!]))\right) \\ & - k_1 \rho^+ c_s^+ \operatorname{sym}\left(\boldsymbol{n} \otimes (\boldsymbol{n} \times (\boldsymbol{n} \times [\boldsymbol{v}]))\right),\end{aligned}$$

and for the velocity equation by

$$\begin{aligned}\boldsymbol{n} \cdot \left[(\mathfrak{F}\mathfrak{q})_{\boldsymbol{v}}^* - (\mathfrak{F}\mathfrak{q})_{\boldsymbol{v}}\right] = {} & \left(k_0 \boldsymbol{n} \cdot [\![\mathsf{C}\boldsymbol{E}]\!] + k_0 \rho^+ c_p^+ [\![\boldsymbol{v}]\!]\right) \rho^- c_p^- \boldsymbol{n} \\ & - k_1 \rho^- c_s^- \boldsymbol{n} \times (\boldsymbol{n} \times [\![\mathsf{C}\boldsymbol{E}]\!]) \\ & - k_1 \rho^+ c_s^+ \rho^- c_s^- \boldsymbol{n} \times (\boldsymbol{n} \times [\boldsymbol{v}]),\end{aligned}$$

with $k_0 = \left(\rho^- c_p^- + \rho^+ c_p^+\right)^{-1}$, $k_1 = \left(\rho^- c_s^- + \rho^+ c_s^+\right)^{-1}$ if $\mu^- \neq 0$, and $k_1 = 0$ if $\mu^- = 0$. Here, we will consider only traction boundary conditions $\boldsymbol{S}\boldsymbol{n} = \boldsymbol{t}_{bc}$, where $\boldsymbol{t}_{bc}$ is the prescribed traction. The traction condition is enforced by the mirror principle,

$$[\![\boldsymbol{v}]\!] = [\boldsymbol{v}] = \boldsymbol{0} \quad \text{and} \quad [\![\boldsymbol{S}]\!] = -2\left(\boldsymbol{t}_{bc} - \boldsymbol{S}^- \boldsymbol{n}\right),$$

which applies to both elastic and acoustic media.

We next specialize (3.1) to the case of Maxwell's equations. In this case,

$$\mathfrak{q} = \begin{pmatrix} \boldsymbol{E} \\ \boldsymbol{H} \end{pmatrix} \in \mathcal{V}, \quad \mathcal{Q} = \begin{pmatrix} \varepsilon \boldsymbol{I} & \boldsymbol{0} \\ \boldsymbol{0} & \mu \boldsymbol{I} \end{pmatrix}, \quad \mathfrak{g} = \begin{pmatrix} \boldsymbol{0} \\ \boldsymbol{0} \end{pmatrix} \in \mathcal{V},$$

where $\boldsymbol{E}$ denotes the electric field, $\boldsymbol{H}$ the magnetic field, μ the permeability, and ε the permittivity.

The action of the flux operator $\mathfrak{F}$ on the electromagnetic field $\mathfrak{q}$ is defined by

$$(\mathfrak{F}\mathfrak{q})_i = \begin{pmatrix} -\boldsymbol{e}_i \times \boldsymbol{H} \\ \boldsymbol{e}_i \times \boldsymbol{E} \end{pmatrix} \in \mathcal{V} \quad \text{for } i = 1, 2, 3,$$

where $\mathcal{V} = \boldsymbol{V}^3$ and $\mathfrak{q}_d|_{\mathsf{D}^e} \circ \boldsymbol{X}^e \in \mathcal{V}_d^e \equiv \mathbb{Q}_{N_e}^3$. The exact Riemann numerical flux for the electric equation can be shown to be [14]

$$\boldsymbol{n} \cdot \left[(\mathfrak{F}\mathfrak{q})^*_{\boldsymbol{E}} - (\mathfrak{F}\mathfrak{q})_{\boldsymbol{E}}\right] = \frac{1}{2\,\{\{Z\}\}} \boldsymbol{n} \times \left(Z^+ [\boldsymbol{H}] - \boldsymbol{n} \times [\boldsymbol{E}]\right),$$

and for the magnetic equation,

$$\boldsymbol{n} \cdot \left[(\mathfrak{F}\mathfrak{q})^*_{\boldsymbol{H}} - (\mathfrak{F}\mathfrak{q})_{\boldsymbol{H}}\right] = -\frac{1}{2\,\{\{Y\}\}} \boldsymbol{n} \times \left(Y^+ [\boldsymbol{E}] + \boldsymbol{n} \times [\boldsymbol{H}]\right),$$

where

$$Z^\pm = \frac{1}{Y^\pm} = \sqrt{\frac{\mu^\pm}{\epsilon^\pm}}.$$

Similarly to the elastic-acoustic coupling case, we use the mirror principle to enforce a perfect electric conductor (PEC) boundary condition by

$$Z^- = Z^+, \quad Y^- = Y^+, \quad \boldsymbol{n} \times [\boldsymbol{H}] = 0, \quad \boldsymbol{n} \times [\boldsymbol{E}] = 2\boldsymbol{n} \times \boldsymbol{E}^-,$$

and a perfect magnetic conductor (PMC) boundary condition by

$$Z^- = Z^+, \quad Y^- = Y^+, \quad \boldsymbol{n} \times [\boldsymbol{E}] = 0, \quad \boldsymbol{n} \times [\boldsymbol{H}] = 2\boldsymbol{n} \times \boldsymbol{H}^-.$$

For dielectric boundary conditions we use

$$\boldsymbol{n} \times \boldsymbol{E}^- = \boldsymbol{n} \times \boldsymbol{E}^+, \quad \boldsymbol{n} \times \boldsymbol{H}^- = \boldsymbol{n} \times \boldsymbol{H}^+.$$

In order to unify the treatment for elastic, acoustic, coupled elastic-acoustic, and electromagnetic waves, we define a generic polynomial space $\mathcal{P}_N$ whose meaning will be clear in each context. For example, if we write $\mathfrak{q}^e \in \mathcal{P}_N$, this identifies $\mathcal{P}_N \equiv \mathcal{V}_d^e$.

The tensor product basis for $\mathbb{Q}_N$ is built upon the one-dimensional Lagrange basis

$$\ell_l(\xi) = \prod_{\substack{k=0,1,\ldots,N \\ k \neq l}} \frac{\xi - \xi_k}{\xi_l - \xi_k},$$

where the Nth-degree Legendre–Gauss–Lobatto (LGL) points, or Nth-degree Legendre–Gauss points (LG), $\{\xi_l\}$ on $[-1, 1]$ for $l = 0, \ldots, N$, are chosen as both the interpolation and quadrature points. This is also known as the collocation approach. The Lagrange interpolant of a function $f(\boldsymbol{r})$ on the reference element $\hat{\mathsf{D}}$ is defined through the interpolation operator $\mathcal{I}_N$ as

$$\mathcal{I}_N(f) = \sum_{l,m,n=0}^{N} f_{lmn} \ell_l(r_1) \ell_m(r_2) \ell_n(r_3), \quad f_{lmn} = f(\boldsymbol{\xi}_{lmn}),$$
$$\boldsymbol{\xi}_{lmn} = (\xi_l, \xi_m, \xi_n) \in \hat{\mathsf{D}}.$$

A typical collocation approach [18] in semidiscretizing (3.1) is as follows. Find $\mathfrak{q} \in \mathcal{V}_d$ such that

$$\begin{aligned}\sum_e \int_{\hat{\mathsf{D}},N_e} \mathcal{I}_{N_e}\left(\mathcal{I}_{N_e}\left(J^e\right)\mathcal{I}_{N_e}\left(\mathcal{Q}^e\right)\frac{\partial \mathfrak{q}^e}{\partial t}\right)\cdot \mathfrak{p}^e\, d\boldsymbol{r} + \int_{\hat{\mathsf{D}},N_e} \nabla_{\boldsymbol{r}}\cdot \mathcal{I}_{N_e}\left(\tilde{\mathfrak{F}}\mathfrak{q}^e\right)\cdot \mathfrak{p}^e\, d\boldsymbol{r} \\ + \int_{\partial\hat{\mathsf{D}},N_e} \tilde{\boldsymbol{n}}\cdot\left[\mathcal{I}_{N_e}\left(\left(\tilde{\mathfrak{F}}\mathfrak{q}^e\right)^*\right) - \mathcal{I}_{N_e}\left(\tilde{\mathfrak{F}}\mathfrak{q}^e\right)\right]\cdot \mathfrak{p}^e\, d\boldsymbol{s} \\ = \sum_e \int_{\hat{\mathsf{D}},N_e} \mathcal{I}_{N_e}\left(\mathcal{I}_{N_e}\left(J^e\right)\mathcal{I}_{N_e}\left(\mathfrak{g}^e\right)\right)\cdot \mathfrak{p}^e\, d\boldsymbol{r} \quad \forall \mathfrak{p}\in\mathcal{V}_d, \end{aligned} \tag{3.2}$$

where $\mathcal{I}_{N_e}(\tilde{\mathfrak{F}}^i) = \mathcal{I}_{N_e}(\mathcal{I}_{N_e}\left(J^e\boldsymbol{a}^i\right)\cdot\mathcal{I}_{N_e}(\mathfrak{F}))$. The direct consequence of the above collocation is that the integrand in each integral is at most of order $2N_e$ in each direction $r_i, i = 1,2,3$. The subscript N_e in the integrals means that the integrals are numerically evaluated using the corresponding N_eth-degree LGL (or LG) quadrature rule.

4. Semidiscrete stability for conforming meshes. In this section, we provide a stability proof for both the elastic-acoustic and electromagnetic cases on conforming meshes. By conforming meshes we mean that the intersection of two elements is either an entire face, an entire edge, or a corner, and that the solution order is the same for all elements. It is sufficient to prove semidiscrete stability since, by a result in [21] (and the references therein), if the semi-discrete equation is stable, the fully discrete system with the time derivative discretized by a locally stable Runge–Kutta (for example, the classical fourth-order Runge–Kutta method) is stable as well, as long as the time step is sufficiently small.

Here, we employ the energy approach to prove stability. For the elastic-acoustic case, the semidiscrete energy functional $\mathcal{E}_d(t)$ is defined as

$$\mathcal{E}_d(t) := \sum_{e=1}^{n_{\mathrm{el}}} \mathcal{E}_d^e(t), \quad \text{where} \quad \mathcal{E}_d^e(t) := \frac{1}{2}\int_{\mathsf{D}^e,N_e} \left(\boldsymbol{E}:(\mathbf{C}\boldsymbol{E}) + \rho\boldsymbol{v}\cdot\boldsymbol{v}\right) d\boldsymbol{x},$$

and for the electromagnetic case as

$$\mathcal{E}_d(t) := \sum_{e=1}^{n_{\mathrm{el}}} \mathcal{E}_d^e(t), \quad \text{where} \quad \mathcal{E}_d^e(t) := \frac{1}{2}\int_{\mathsf{D}^e,N_e} \left(\epsilon\boldsymbol{E}\cdot\boldsymbol{E} + \mu\boldsymbol{H}\cdot\boldsymbol{H}\right) d\boldsymbol{x}.$$

For convenience, we define the elementwise discrete L^2 inner product and the induced norm on a generic domain D, which could be an element or its boundary, as

$$(\mathfrak{q},\mathfrak{p})_{D,N} = \int_{D,N} \mathfrak{q}\cdot\mathfrak{p}\, d\boldsymbol{x}, \quad \|\mathfrak{q}\|_{D,N}^2 = \int_{D,N} \mathfrak{q}\cdot\mathfrak{q}\, d\boldsymbol{x},$$

and their continuous counterparts as

$$(\mathfrak{q},\mathfrak{p})_{D} = \int_{D} \mathfrak{q}\cdot\mathfrak{p}\, d\boldsymbol{x}, \quad \|\mathfrak{q}\|_{D}^2 = \int_{D} \mathfrak{q}\cdot\mathfrak{p}\, d\boldsymbol{x}.$$

The discrete global L^2 norm is computed as the summation of the elementwise contributions

$$\|\mathfrak{q}\|_{\mathcal{D}^{n_{\mathrm{el}}},d}^2 = \sum_e \|\mathfrak{q}\|_{\mathsf{D}^e,N_e}^2 .$$

THEOREM 1 (stability for conforming meshes). *Assume that the mesh is affine and conforming with solution order N; then the DGSEM discretization is stable in the following sense:*

$$\frac{d}{dt}\mathcal{E}_d \leq \frac{1}{2}\left(\mathcal{E}_d + \|\mathcal{I}_N \mathfrak{g}\|^2_{\mathcal{D}^{n_{el}},d}\right).$$

Moreover, if $\mathfrak{g} = 0$, then $\frac{d}{dt}\mathcal{E}_d \leq 0$.

Proof. Substituting $\mathfrak{p} := \binom{\boldsymbol{S}}{\boldsymbol{v}} := \binom{\mathbf{C}\boldsymbol{E}}{\boldsymbol{v}}$ for the elastic-acoustic coupling case and $\mathfrak{p} = \mathfrak{q}$ for the electromagnetic case into (3.2), and using a discrete integration by parts formula [26, 19], we obtain

$$\begin{aligned}\sum_e \frac{d}{dt}\mathcal{E}_d^e = \frac{1}{2}\sum_e \int_{\hat{\mathsf{D}},N} \left[\mathcal{I}_N\left(\tilde{\mathfrak{F}}\mathfrak{q}^e\right)\cdot\nabla_{\boldsymbol{r}}\cdot\mathfrak{p}^e - \nabla_{\boldsymbol{r}}\cdot\mathcal{I}_N\left(\tilde{\mathfrak{F}}\mathfrak{q}^e\right)\cdot\mathfrak{p}^e\right] d\boldsymbol{r} \\ - \int_{\partial\hat{\mathsf{D}},N} \tilde{\boldsymbol{n}}\cdot\left[\left(\tilde{\mathfrak{F}}\mathfrak{q}^e\right)^* - \frac{1}{2}\tilde{\mathfrak{F}}\mathfrak{q}^e\right]\cdot\mathfrak{p}^e\, d\boldsymbol{s} + \int_{\hat{\mathsf{D}},N} J^e\mathfrak{g}^e\cdot\mathfrak{p}^e\, d\boldsymbol{r},\end{aligned} \tag{4.1}$$

where we have dropped the interpolation operator $\mathcal{I}_{N_e}$ in the last two terms on the right-hand side of (4.1) since the interpolation is an orthogonal projection with the discrete L^2 inner product [8], e.g.,

$$\int_{D,N} qp\, d\boldsymbol{x} = \int_{D,N} \mathcal{I}_N(q)\, p\, d\boldsymbol{x}. \tag{4.2}$$

For affine meshes, the metric terms $J^e\boldsymbol{a}^i, i = 1,2,3$, are constant, and thus

$$\mathcal{I}_N\left(\tilde{\mathfrak{F}}^i\right) = J^e\boldsymbol{a}^i\cdot\mathcal{I}_N(\mathfrak{F}).$$

After some simple manipulations, for either the elastic-acoustic case or the electromagnetic case, one has

$$\int_{\hat{\mathsf{D}},N}\left(\mathcal{I}_N\left(\tilde{\mathfrak{F}}\mathfrak{q}^e\right)\cdot\nabla_{\boldsymbol{r}}\mathfrak{p}^e - \nabla_{\boldsymbol{r}}\cdot\mathcal{I}_N\left(\tilde{\mathfrak{F}}\mathfrak{q}^e\right)\cdot\mathfrak{p}^e\right) d\boldsymbol{r} = 0.$$

As a result, the volume terms vanish and the preceding equation can be expressed in the integrals over physical space as

$$\sum_e \frac{d}{dt}\mathcal{E}_d^e = -\sum_e \int_{\partial\mathsf{D}^e,N} \boldsymbol{n}\cdot\left[(\mathfrak{F}\mathfrak{q}^e)^* - \frac{1}{2}\mathfrak{F}\mathfrak{q}^e\right]\cdot\mathfrak{p}^e\, d\boldsymbol{s} + \int_{\mathsf{D}^e,N}\mathfrak{g}^e\cdot\mathfrak{p}^e\, d\boldsymbol{x}. \tag{4.3}$$

Next, if $\partial\mathsf{D}^e \cap \partial\mathsf{D}^{e'}$ is a nonempty two-dimensional intersection ($\partial\mathsf{D}^e \cap \partial\mathsf{D}^{e'}$ has nonzero two-dimensional Lebesgue measure), we combine the integrands of the surface integrals on both "$-$" and "$+$" LGL (or LG) points. This is possible due to the mesh conformity; i.e., the number of LGL (or LG) points on "$-$" and "$+$" sides are the same and they can be reordered to be exactly coincident. After some algebraic manipulations for the surface integrals on the right-hand side of (4.3), the following holds for the elastic-acoustic case:

$$\begin{aligned}\sum_e \frac{d}{dt}\mathcal{E}_d^e = -\frac{1}{2}\sum_e \int_{\partial\mathsf{D}^e,N} k_0\left\{(\boldsymbol{n}\cdot[\![\boldsymbol{S}]\!])^2 + \rho^-c_p^-\rho^+c_p^+[\![\boldsymbol{v}]\!]^2\right\} \\ + k_1\left\{\|\boldsymbol{n}\times(\boldsymbol{n}\times[\![\boldsymbol{S}]\!])\|^2 + \rho^-c_s^-\rho^+c_s^+\|\boldsymbol{n}\times(\boldsymbol{n}\times[\boldsymbol{v}])\|^2\right\} d\boldsymbol{s} \\ + \int_{\mathsf{D}^e,N}\mathfrak{g}^e\cdot\mathfrak{p}^e\, d\boldsymbol{x},\end{aligned}$$

where terms involving k_1 are zero for a face either on or adjacent to the acoustic side. Similarly, for the electromagnetic case

$$\sum_e \frac{d}{dt}\mathcal{E}_d^e = \sum_e \int_{\mathsf{D}^e,N} \mathfrak{g}^e \cdot \mathfrak{p}^e \, d\boldsymbol{x} \\ -\frac{1}{2}\int_{\partial\mathsf{D}^e,N} \frac{1}{2\,\{\{Z\}\}} \|\boldsymbol{n}\times\boldsymbol{n}\times[\boldsymbol{E}]\|^2 + \frac{1}{2\,\{\{Y\}\}} \|\boldsymbol{n}\times\boldsymbol{n}\times[\boldsymbol{H}]\|^2 \, d\boldsymbol{s},$$

where terms involving $\boldsymbol{E}$ and $\boldsymbol{H}$ vanish for PMC and PEC boundaries, respectively, and both vanish for dielectric boundaries.

Now, for $\mathfrak{g} = 0$ the overall energy is nonincreasing, i.e.,

$$\frac{d}{dt}\mathcal{E}_d \le 0.$$

For $\mathfrak{g} \neq 0$, we obtain the following estimate by the Cauchy–Schwarz and Young inequalities:

$$\frac{d}{dt}\mathcal{E}_d \le \int_{\mathcal{D}^{n_{\mathrm{el}}}} \mathfrak{g}\cdot\mathfrak{p} \le \frac{1}{2}\left(\mathcal{E}_d + \|\mathcal{I}_N \boldsymbol{g}\|^2_{\mathcal{D}^{n_{\mathrm{el}}},d}\right). \qquad \square$$

5. Mortar-based nonconforming approximations. In this section, we employ the mortar-based approximation idea proposed by Kopriva [16] and Kopriva, Woodruff, and Hussaini [20]. However, we propose to use a discretized mortar-based approximation to show stability in addition to the outflow condition and global conservation required by the original mortar method [16, 20]. As will be shown, our discrete version requires an adaptive quadrature rule in order to simultaneously satisfy all the requirements. We provide a setting that allows unified proofs that are valid for both functional (due to order refinement) and geometric (due to local subdivision) nonconforming approximations.

The following conventions are adopted. We use boldface type to denote vectors of nodal values of the corresponding quantities under consideration. For example, $\mathbf{q}$ is the vector of nodal values of $\mathfrak{q}$. In addition, we use upper case script type to denote matrices, e.g., $\mathscr{P}$.

We consider nonconforming approximations due to domain subdivision in which elements may be subdivided locally, while their neighbors may not. For simplicity of exposition, we further restrict ourselves to the case where a subdomain interface between two adjacent elements (two elements are said to be *adjacent* to each other if their boundary intersection has nonzero two-dimensional Lebesgue measure) must be an entire face of either of them. (The case of fully h-nonconforming interfaces in which faces of contributing elements partially overlap with each other is treated similarly [16].) Nevertheless, adjacent elements are allowed to have different solution orders, and hence order refinement (i.e., p-refinement) in addition to domain subdivision (i.e., h-refinement) is permissible. From here on, by "nonconforming interface" we mean that an entire face of one element is also a union of faces of other adjacent elements (h-nonconforming) or the solution orders of two elements sharing a face are different (p-nonconforming). A nonconforming interface with one element on one side and seven elements on the other side is shown in Figure 5.1.

Consider a nonconforming interface where on the "$-$" side is face f_{e_0} of element e_0 and on the "$+$" side are faces f_{e_i} of elements $e_i, i = 1, \ldots, N_a$. Clearly, this setting includes both kinds of nonconforming interfaces. We create N_a mortars $\mathcal{M}_i, i =$

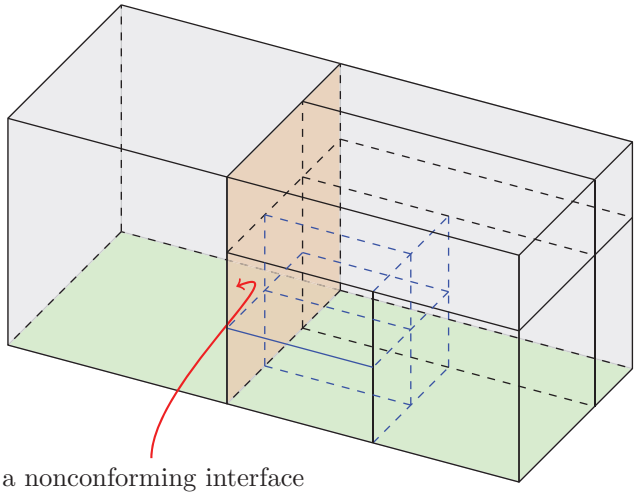

FIG. 5.1. *A nonconforming interface with one hexahedron on one side and seven hexahedra on the other side.*

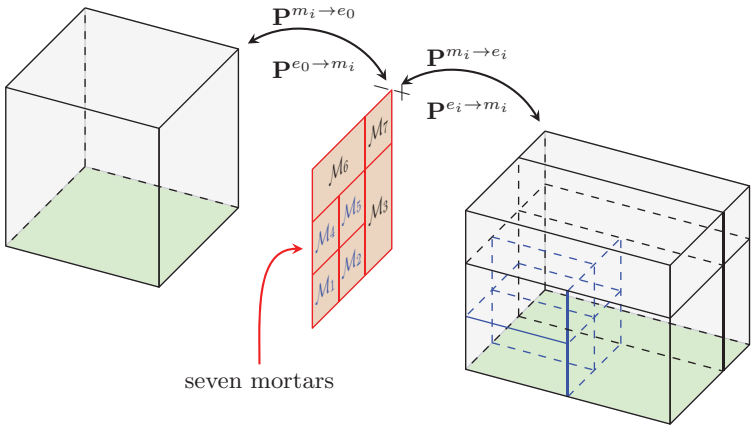

FIG. 5.2. *Seven mortars corresponding to the nonconforming interface in Figure* 5.1.

$1, \ldots, N_a$, whose "$-$" sides are seen by element e_0 and "$+$" sides by elements e_i, respectively. As in [20], the geometric order on the mortars must be the lowest geometric order of the contributing elements, and the polynomial should be defined along face f_{e_0}. This will ensure that the mortars match subinterfaces between elements exactly, and hence the metrics $J^{e_i}\boldsymbol{a}^{e_i}$ on a mortar and the corresponding contributing element faces are represented by identical polynomials. The solution orders of the mortars are chosen as $N_{m_i} \geq \max\{N_{e_0}, N_{e_i}\}$, which is sufficient to satisfy the outflow condition, as we shall show. An example with seven mortars corresponding to the nonconforming interface in Figure 5.1 is shown in Figure 5.2.

The goal of the mortar approximation is to compute the contravariant fluxes on faces $f_{e_i}, i = 0, \ldots, N_a$. This is a three-step process. First, the states on e_0 and e_i are projected onto the mortars through L^2 projectors $\mathscr{P}^{e_0 \to m_i}$ and $\mathscr{P}^{e_i \to m_i}$, $i = 1, \ldots, N_a$. The projected states are then used to compute the mortar contravariant fluxes as if each mortar is a conforming face. The final step is to project the con-

travariant fluxes back onto the element faces using projectors $\mathscr{P}^{m_i \to e_0}$ and $\mathscr{P}^{m_i \to e_i}$. The illustration of steps 1 and 3 can be seen in Figure 5.2. The components of each step are now detailed.

State $\mathfrak{q}^{m_i^-}$ on the "$-$" side of mortar $\mathcal{M}_i$ is the least-squares projection of state $\mathfrak{q}^{e_0}$ from element e_0 onto space $\mathcal{P}_{N_{m_i}}$, i.e.,

$$\begin{aligned}&\int_{\mathcal{M}_i} \mathfrak{q}^{m_i^-}(\boldsymbol{r})\, \boldsymbol{\ell}_k^{m_i}(\boldsymbol{r})\, d\boldsymbol{s}\\ &\quad = \int_{\mathcal{M}_i} \mathfrak{q}^{e_0}\left((\boldsymbol{X}^{e_0})^{-1} \circ \boldsymbol{X}^{e_i}(\boldsymbol{r})\right) \boldsymbol{\ell}_k^{m_i}(\boldsymbol{r})\, d\boldsymbol{s} \quad \forall \boldsymbol{\ell}_k^{m_i}(\boldsymbol{r}) \in \mathcal{P}_{N_{m_i}}.\end{aligned} \tag{5.1}$$

Since our main goal is to prove semistability, least-squares projection of the type (5.1) is approximated using quadratures. Nevertheless, we do not wish to violate the outflow condition and global conservation. In fact, the outflow condition is necessary to ensure stability, as shown in section 6. In this paper, the following adaptive quadrature rule is used. For any surface integral in the least-squares projection of type (5.1), the quadrature rule is chosen to correspond to the integrand with the highest order. For example, the N_{m_i}th-order quadrature rule is used for both integrals in (5.1). Explicitly, we approximate (5.1) as

$$\begin{aligned}&\int_{\mathcal{M}_i, N_{m_i}} \mathfrak{q}^{m_i^-}(\boldsymbol{r})\, \boldsymbol{\ell}_k^{m_i}(\boldsymbol{r})\, d\boldsymbol{s}\\ &\quad = \int_{\mathcal{M}_i, N_{m_i}} \mathfrak{q}^{e_0}\left((\boldsymbol{X}^{e_0})^{-1} \circ \boldsymbol{X}^{e_i}(\boldsymbol{r})\right) \boldsymbol{\ell}_k^{m_i}(\boldsymbol{r})\, d\boldsymbol{s} \quad \forall \boldsymbol{\ell}_k^{m_i}(\boldsymbol{r}) \in \mathcal{P}_{N_{m_i}},\end{aligned} \tag{5.2}$$

which yields

$$\mathbf{q}^{m_i^-} = \underbrace{(\mathscr{M}^{m_i})^{-1} \mathscr{R}^{e_0 \to m_i}}_{\mathscr{P}^{e_0 \to m_i}} \mathbf{q}^{e_0},$$

where the matrices $\mathscr{M}^{m_i}$ and $\mathscr{R}^{e_0 \to m_i}$ are defined as

$$\begin{aligned}\mathscr{M}^{m_i}_{k_1,k_2} &= \int_{\mathcal{M}_i, N_{m_i}} \boldsymbol{\ell}_{k_1}^{m_i}(\boldsymbol{r})\, \boldsymbol{\ell}_{k_2}^{m_i}(\boldsymbol{r})\, d\boldsymbol{s},\\ \mathscr{R}^{e_0 \to m_i}_{k,j} &= \int_{\mathcal{M}_i, N_{m_i}} \boldsymbol{\ell}_k^{m_i}(\boldsymbol{r})\, \boldsymbol{\ell}_j^{e_0}\left((\boldsymbol{X}^{e_0})^{-1} \circ \boldsymbol{X}^{e_i}(\boldsymbol{r})\right) d\boldsymbol{s} \quad \forall \boldsymbol{\ell}_j^{e_0} \in \mathcal{P}_{N_{e_0}}.\end{aligned}$$

Similarly, the least-squares projection of state $\mathfrak{q}^{e_i}$ from element e_i onto $\mathcal{P}_{N_{m_i}}$ is state $\mathfrak{q}^{m_i^+}$ on the "$+$" side of mortar $\mathcal{M}_i$. Using the above quadrature rule we have

$$\int_{\mathcal{M}_i, N_{m_i}} \mathfrak{q}^{m_i^+}(\boldsymbol{r})\, \boldsymbol{\ell}_k^{m_i}(\boldsymbol{r})\, d\boldsymbol{s} = \int_{\mathcal{M}_i, N_{m_i}} \mathfrak{q}^{e_i}(\boldsymbol{r})\, \boldsymbol{\ell}_k^{m_i}(\boldsymbol{r})\, d\boldsymbol{s} \quad \forall \boldsymbol{\ell}_k^{m_i}(\boldsymbol{r}) \in \mathcal{P}_{N_{m_i}} \tag{5.3}$$

or, equivalently,

$$\mathbf{q}^{m_i^+} = \underbrace{(\mathscr{M}^{m_i})^{-1} \mathscr{R}^{e_i \to m_i}}_{\mathscr{P}^{e_i \to m_i}} \mathbf{q}^{e_i} \tag{5.4}$$

with $\mathscr{R}^{e_i \to m_i}$ defined as

$$\mathscr{R}^{e_i \to m_i}_{k,j} = \int_{\mathcal{M}_i, N_{m_i}} \boldsymbol{\ell}_k^{m_i}(\boldsymbol{r})\, \boldsymbol{\ell}_j^{e_i}(\boldsymbol{r})\, d\boldsymbol{s} \quad \forall \boldsymbol{\ell}_j^{e_i} \in \mathcal{P}_{N_{e_i}}.$$

Since the fluxes depend on $\lambda, \mu, \varepsilon$, and μ, we perform the above least-squares projection procedure on them as well. Based on the projected states $\mathfrak{q}^{m_i^-}$, $\mathfrak{q}^{m_i^+}$ and projected coefficients, we compute the contravariant Riemann fluxes $\tilde{\mathfrak{F}}^*_{m_i} = (\tilde{\boldsymbol{n}} \cdot \tilde{\mathfrak{F}}(\mathfrak{q}^{m_i}))^*$ on the mortars as if the mortars are conforming faces. This is done using a simple relation between the contravariant and covariant Riemann fluxes as in [18]. The projected states are also used to compute the contravariant fluxes $\tilde{\mathfrak{F}}^-_{m_i} = \tilde{\boldsymbol{n}} \cdot \tilde{\mathfrak{F}}(\mathfrak{q}^{m_i^-})$ and $\tilde{\mathfrak{F}}^+_{m_i} = \tilde{\boldsymbol{n}} \cdot \tilde{\mathfrak{F}}(\mathfrak{q}^{m_i^+})$. The final step is to project the mortar contravariant fluxes $\tilde{\mathfrak{F}}^*_{m_i}, \tilde{\mathfrak{F}}^-_{m_i}$ and $\tilde{\mathfrak{F}}^+_{m_i}$ onto $\mathcal{P}_{N_{e_i}}, i = 0, \ldots, N_a$. Since the procedure is the same for $\tilde{\mathfrak{F}}^*_{m_i}, \tilde{\mathfrak{F}}^-_{m_i}$, and $\tilde{\mathfrak{F}}^+_{m_i}$, we describe only the process of projecting $\tilde{\mathfrak{F}}^*_{m_i}$ to obtain the contravariant fluxes $\tilde{\mathfrak{F}}^*_{e_i}$ on faces f_{e_i} of the contributing elements. The discretized least-squares projection using the quadrature rule discussed above for face f_{e_0} is as follows:

$$\begin{aligned}
&\int_{f_{e_0}, N_{e_0}} \tilde{\mathfrak{F}}^*_{e_0}(\boldsymbol{r})\, \boldsymbol{\ell}_j^{e_0}(\boldsymbol{r})\, d\boldsymbol{s} \\
&= \sum_{i=1}^{N_a} \int_{\mathcal{M}_i, N_{m_i}} \tilde{\mathfrak{F}}^*_{m_i}(\boldsymbol{r})\, \boldsymbol{\ell}_j^{e_0}\left(\left(\boldsymbol{X}^{e_0}\right)^{-1} \circ \boldsymbol{X}^{e_i}(\boldsymbol{r}) \right) d\boldsymbol{s} \quad \forall \boldsymbol{\ell}_j^{e_0} \in \mathcal{P}_{N_{e_0}}
\end{aligned} \tag{5.5}$$

for which, in matrix notation, the vector of nodal values of $\tilde{\mathfrak{F}}^*_{e_0}$, $\tilde{\mathbf{F}}^*_{e_0}$, is computed as

$$\mathscr{M}^{e_0} \tilde{\mathbf{F}}^*_{e_0} = \sum_{i=1}^{N_a} \mathscr{R}^{m_i \to e_0} \tilde{\mathbf{F}}^*_{m_i}$$

or, in terms of projection matrices,

$$\tilde{\mathbf{F}}^*_{e_0} = \sum_{i=1}^{N_a} \underbrace{\left(\mathscr{M}^{e_0}\right)^{-1} \mathscr{R}^{m_i \to e_0}}_{\mathscr{P}^{m_i \to e_0}} \tilde{\mathbf{F}}^*_{m_i}, \tag{5.6}$$

where

$$\mathscr{M}^{e_0}_{k,j} = \int_{\mathcal{M}_i, N_{e_0}} \boldsymbol{\ell}_k^{e_0}(\boldsymbol{r})\, \boldsymbol{\ell}_j^{e_0}(\boldsymbol{r})\, d\boldsymbol{s}, \quad \mathscr{R}^{m_i \to e_0} = \left(\mathscr{R}^{e_0 \to m_i}\right)^T. \tag{5.7}$$

Similarly, the vector of nodal values of $\tilde{\mathfrak{F}}^-_{e_0}$, $\tilde{\mathbf{F}}^-_{e_0}$, is given by

$$\tilde{\mathbf{F}}^-_{e_0} = \sum_{i=1}^{N_a} \mathscr{P}^{m_i \to e_0} \tilde{\mathbf{F}}^-_{m_i}. \tag{5.8}$$

The projection to compute contravariant fluxes $\tilde{\mathfrak{F}}^*_{e_i}$ on surface f_{e_i}, $i = 1, \ldots, N_a$, of other contributing elements is simpler,

$$\int_{\mathcal{M}_i, N_{e_i}} \tilde{\mathfrak{F}}^*_{e_i}(\boldsymbol{r})\, \boldsymbol{\ell}_j^{e_i}(\boldsymbol{r})\, d\boldsymbol{s} = \int_{\mathcal{M}_i, N_{m_i}} \tilde{\mathfrak{F}}^*_{m_i}(\boldsymbol{r})\, \boldsymbol{\ell}_j^{e_i}(\boldsymbol{r})\, d\boldsymbol{s} = 0 \quad \forall \boldsymbol{\ell}_j^{e_i}(\boldsymbol{r}) \in \mathcal{P}_{N_{e_i}}, \tag{5.9}$$

which yields

$$\tilde{\mathbf{F}}^*_{e_i} = \underbrace{\left(\mathscr{M}^{e_i}\right)^{-1} \mathscr{R}^{m_i \to e_i}}_{\mathscr{P}^{m_i \to e_i}} \tilde{\mathbf{F}}^*_{m_i}, \tag{5.10}$$

where

$$\mathscr{M}_{k,j}^{e_i} = \int_{\mathcal{M}_i, N_{e_i}} \boldsymbol{\ell}_k^{e_i}(\boldsymbol{r})\, \boldsymbol{\ell}_j^{e_i}(\boldsymbol{r})\, d\boldsymbol{s}, \quad \mathscr{R}^{m_i \to e_i} = \left(\mathscr{R}^{e_i \to m_i}\right)^T. \tag{5.11}$$

Similarly,

$$\tilde{\mathbf{F}}_{e_i}^{+} = \mathscr{P}^{m_i \to e_i} \tilde{\mathbf{F}}_{m_i}^{+}. \tag{5.12}$$

Recall that the outflow condition means the invariance of a polynomial function when projected to the mortars and back to the face [16, 20]. We are now in a position to discuss the outflow condition for the above discrete mortar-based approximation.

PROPOSITION 1 (outflow condition). *Assume* $N_{m_i} \geq \max\{N_{e_0}, N_{e_i}\}$, $i = 1, \ldots, N_a$. *Then the discrete mortar-based approximation with LG quadrature satisfies the strong outflow conditions, namely,*

$$\mathscr{P}^{m_i \to e_i} \mathscr{P}^{e_i \to m_i} = \boldsymbol{I}, \quad i = 1, \ldots, N_a, \tag{5.13}$$

$$\sum_{i=1}^{N_a} \mathscr{P}^{m_i \to e_0} \mathscr{P}^{e_0 \to m_i} = \boldsymbol{I}, \tag{5.14}$$

where $\boldsymbol{I}$ *is the identity matrix of appropriate size. On the other hand, discretizations using LGL quadrature satisfy the outflow condition in the following weak sense:*

$$\int_{\mathcal{M}_i, N_{m_i}} \mathfrak{q}^{e_i}(\boldsymbol{r})\, \hat{\boldsymbol{\ell}}\, d\boldsymbol{s} = \int_{\mathcal{M}_i, N_{e_i}} \hat{\mathfrak{q}}^{e_i}(\boldsymbol{r})\, \hat{\boldsymbol{\ell}}\, d\boldsymbol{s} \quad \forall \hat{\boldsymbol{\ell}} \in \mathcal{P}_{N_{e_i}}, \tag{5.15}$$

and

$$\begin{aligned} \sum_{i=1}^{N_a} \int_{\mathcal{M}_i, N_{m_i}} \mathfrak{q}^{e_0}\left(\left(\boldsymbol{X}^{e_0}\right)^{-1} \circ \boldsymbol{X}^{e_i}(\boldsymbol{r})\right) \hat{\boldsymbol{\ell}}\left(\left(\boldsymbol{X}^{e_0}\right)^{-1} \circ \boldsymbol{X}^{e_i}(\boldsymbol{r})\right) d\boldsymbol{s} \\ = \int_{f_{e_0}, N_{e_0}} \hat{\mathfrak{q}}^{e_0}(\boldsymbol{r})\, \hat{\boldsymbol{\ell}}(\boldsymbol{r})\, d\boldsymbol{s} \quad \forall \hat{\boldsymbol{\ell}} \in \mathcal{P}_{N_{e_0}}, \end{aligned} \tag{5.16}$$

where $\hat{\mathfrak{q}}^{e_i}$ *is the result from the projection of* $\mathfrak{q}^{e_i}$ *onto* $\mathcal{M}_i$ *and back onto* f_{e_i}, *and* $\hat{\mathfrak{q}}^{e_0}$ *the result from the projection of* $\mathfrak{q}^{e_0}$ *onto* $\mathcal{M}_i$ *and back onto* f_{e_0}.

Proof. We first show (5.13). Denoting $\mathbf{q}^{m_i^+}$ as the projection of $\mathbf{q}^{e_i}$ onto mortar $\mathcal{M}_i$, using (5.3) and (5.9), we have

$$\begin{aligned} \int_{\mathcal{M}_i, N_{m_i}} \mathfrak{q}^{m_i^+}(\boldsymbol{r})\, \boldsymbol{\ell}(\boldsymbol{r})\, d\boldsymbol{s} &= \int_{\mathcal{M}_i, N_{m_i}} \mathfrak{q}^{e_i}(\boldsymbol{r})\, \boldsymbol{\ell}(\boldsymbol{r})\, d\boldsymbol{s} \quad \forall \boldsymbol{\ell} \in \mathcal{P}_{N_{m_i}}, \\ \int_{\mathcal{M}_i, N_{m_i}} \mathfrak{q}^{m_i^+}(\boldsymbol{r})\, \hat{\boldsymbol{\ell}}(\boldsymbol{r})\, d\boldsymbol{s} &= \int_{\mathcal{M}_i, N_{e_i}} \hat{\mathfrak{q}}^{e_i}(\boldsymbol{r})\, \hat{\boldsymbol{\ell}}(\boldsymbol{r})\, d\boldsymbol{s} \quad \forall \hat{\boldsymbol{\ell}} \in \mathcal{P}_{N_{e_i}} \subset \mathcal{P}_{N_{m_i}}, \end{aligned}$$

which imply the weak outflow condition (5.15). This weak outflow condition is valid for both LGL and LG quadrature rules. For LG quadrature, however, the weak outflow condition also implies the strong one, namely, $\hat{\mathbf{q}}^{e_i} = \mathbf{q}^{e_i}$, and hence (5.13), since LG quadrature is exact.

For (5.14), denote $\hat{\mathfrak{q}}^{m_i^-}$ as the projection of $\mathfrak{q}^{e_0}$ onto mortars $\mathcal{M}_i$. Equations (5.2) and (5.5) imply, for $i = 1, \ldots, N_a$,

$$\begin{aligned}
&\int_{\mathcal{M}_i, N_{m_i}} \mathfrak{q}^{m_i^-}(\boldsymbol{r})\, \boldsymbol{\ell}(\boldsymbol{r})\, d\boldsymbol{s} \\
&= \int_{\mathcal{M}_i, N_{m_i}} \mathfrak{q}^{e_0}\left((\boldsymbol{X}^{e_0})^{-1} \circ \boldsymbol{X}^{e_i}(\boldsymbol{r})\right) \boldsymbol{\ell}(\boldsymbol{r})\, d\boldsymbol{s} \quad \forall \boldsymbol{\ell} \in \mathcal{P}_{N_{m_i}}, \qquad (5.17)\\
&\sum_{j=1}^{N_a} \int_{\mathcal{M}_j, N_{m_j}} \mathfrak{q}^{m_j^-}(\boldsymbol{r})\, \hat{\boldsymbol{\ell}}\left((\boldsymbol{X}^{e_0})^{-1} \circ \boldsymbol{X}^{e_j}(\boldsymbol{r})\right) d\boldsymbol{s} \\
&= \int_{f_{e_0}, N_{e_0}} \hat{\mathfrak{q}}^{e_0}(\boldsymbol{r})\, \hat{\boldsymbol{\ell}}(\boldsymbol{r})\, d\boldsymbol{s} \quad \forall \hat{\boldsymbol{\ell}} \in \mathcal{P}_{N_{e_0}}. \qquad (5.18)
\end{aligned}$$

Since $N_{m_i} \geq \max\{N_{e_0}, N_{e_i}\}$ and hence $\mathcal{P}_{N_{e_0}} \subset \mathcal{P}_{N_{m_i}}$, $i = 1, \ldots, N_a$, we take $\boldsymbol{\ell}(\boldsymbol{r}) = \hat{\boldsymbol{\ell}}((\boldsymbol{X}^{e_0})^{-1} \circ \boldsymbol{X}^{e_i}(\boldsymbol{r}))$ in (5.17) and sum over $i = 1, \ldots, N_a$, and finally subtract from (5.18) to obtain the weak outflow condition (5.17). Again, by the exactness of LG quadrature we have $\hat{\mathbf{q}}^{e_0} = \mathbf{q}^{e_0}$ and hence (5.14). ∎

Remark 1. It is clear that if $N_{m_i} = N_{e_0} = N_{e_i}$, i.e., only h nonconformity is considered, the weak outflow conditions are indeed strong.

PROPOSITION 2 (global conservation). *The discrete mortar-based approximation satisfies the following global conservation:*

$$\int_{f_{e_0}} \tilde{\mathfrak{F}}^*_{e_0}\, d\boldsymbol{r} = \sum_{i=1}^{N_a} \int_{f_{e_i}} \tilde{\mathfrak{F}}^*_{e_i}\, d\boldsymbol{r}.$$

Proof. This result is an easy consequence of (5.5) and (5.9). Indeed, taking $\boldsymbol{\ell}^{e_0} \equiv 1$ in (5.5) and $\boldsymbol{\ell}_j^{e_i} \equiv 1$ in (5.9), we have

$$\int_{f_{e_0}, N_{e_0}} \tilde{\mathfrak{F}}^*_{e_0}(\boldsymbol{r})\, d\boldsymbol{s} = \sum_{i=1}^{N_a} \int_{\mathcal{M}_i, N_{m_i}} \tilde{\mathfrak{F}}^*_{m_i}(\boldsymbol{r})\, d\boldsymbol{s}$$

and

$$\sum_{i=1}^{N_a} \int_{\mathcal{M}_i, N_{e_i}} \tilde{\mathfrak{F}}^*_{e_i}(\boldsymbol{r})\, d\boldsymbol{s} = \sum_{i=1}^{N_a} \int_{\mathcal{M}_i, N_{m_i}} \tilde{\mathfrak{F}}^*_{m_i}(\boldsymbol{r})\, d\boldsymbol{s}.$$

Observe that $\tilde{\mathfrak{F}}^*_{e_0}(\boldsymbol{r})$ is a polynomial of order at most N_{e_0}, while $\tilde{\mathfrak{F}}^*_{e_i}(\boldsymbol{r})$ is a polynomial of order at most N_{e_i}. The exactness of either LGL or LG quadrature completes the proof. ∎

6. Semidiscrete stability for nonconforming meshes. We start this section with a discussion on why the outflow condition is necessary for the stability proof to hold. The semidiscrete form (3.2) is also applied for nonconforming approximation using the mortar method in section 5. However, the contravariant fluxes $(\tilde{\mathfrak{F}}\mathfrak{q}^e)^*$ and $\tilde{\mathfrak{F}}\mathfrak{q}^e$ on the boundary $\partial\hat{\mathsf{D}}$ are the projected values of the mortar contravariant fluxes instead of the trace of the flux, $\tilde{\mathfrak{F}}\mathfrak{q}^e|_{\partial\hat{\mathsf{D}}}$. Accordingly, using commutativity of quadrature

and integration by parts [26, 19], (3.2) becomes

$$\sum_e \int_{\hat{\mathsf{D}},N_e} J^e \mathcal{Q}^e \frac{\partial \mathfrak{q}^e}{\partial t} \cdot \mathfrak{p}^e \, d\boldsymbol{r} - \int_{\hat{\mathsf{D}},N_e} \mathcal{I}_{N_e} \left(\tilde{\mathfrak{F}} \mathfrak{q}^e \right) \cdot \nabla_{\boldsymbol{r}} \cdot \mathfrak{p}^e \, d\boldsymbol{r}$$
$$+ \int_{\partial \hat{\mathsf{D}},N_e} \tilde{\boldsymbol{n}} \cdot \left[\left(\tilde{\mathfrak{F}} \mathfrak{q}^e \right)^* - \tilde{\mathfrak{F}} \mathfrak{q}^e + \left. \tilde{\mathfrak{F}} \mathfrak{q}^e \right|_{\partial \hat{\mathsf{D}}} \right] \cdot \mathfrak{p}^e \, d\boldsymbol{s} = \sum_e \int_{\hat{\mathsf{D}},N_e} J^e \mathfrak{g}^e \cdot \mathfrak{p}^e \, d\boldsymbol{r}. \tag{6.1}$$

For the conforming approximation, one has $\tilde{\mathfrak{F}} \mathfrak{q}^e|_{\partial \hat{\mathsf{D}}} - \tilde{\mathfrak{F}} \mathfrak{q}^e = 0$ for all $\boldsymbol{r} \in \partial \hat{\mathsf{D}}$, and this is the reason (4.1) holds. This no longer holds for the nonconforming approximation unless $\tilde{\mathfrak{F}} \mathfrak{q}^e = \tilde{\mathfrak{F}} \mathfrak{q}^e|_{\partial \hat{\mathsf{D}}}$ for all $\boldsymbol{r} \in \partial \hat{\mathsf{D}}$, which is true if the outflow condition is satisfied and $\tilde{\mathfrak{F}} \mathfrak{q}^e \in \mathcal{P}_{N_e}$. A sufficient condition for $\tilde{\mathfrak{F}} \mathfrak{q}^e \in \mathcal{P}_{N_e}$ to hold is that the medium properties, i.e., λ, μ, and ε, are elementwise constant.

We introduce the global interpolation operator Π whose restriction on element D^e is

$$\Pi|_{\mathsf{D}^e} = \mathcal{I}_{N_e},$$

which allows us to obtain the following stability proof for our nonconforming approximation. The strategy of our proof is to convert nonconforming computations to equivalent conforming ones for which the stability result is available by Theorem 1.

THEOREM 2 (stability for nonconforming meshes with LG quadratures). *Assume that the following hold:*

(i) *The discrete mortar approach in section* 5 *is used for nonconforming approximations.*

(ii) *The mesh is affine.*

(iii) *The LG quadrature is used; i.e., the strong outflow condition is satisfied.*

(iv) λ, μ, *and* ε *are elementwise constant.*

Then the DGSEM discretization is stable in the sense that

$$\frac{d}{dt} \mathcal{E}_d \leq \frac{1}{2} \left(\mathcal{E}_d + \|\Pi \mathfrak{g}\|^2_{\mathcal{D}^{n_{el}},d} \right).$$

Moreover, if $\mathfrak{g} = 0$, *then* $\frac{d}{dt} \mathcal{E}_d \leq 0$.

Proof. As discussed above, assumptions (iii) and (iv) imply the identity $\tilde{\mathfrak{F}} \mathfrak{q}^e|_{\partial \hat{\mathsf{D}}} - \tilde{\mathfrak{F}} \mathfrak{q}^e = 0$ for all $\boldsymbol{r} \in \partial \hat{\mathsf{D}}$. Therefore, similarly to the proof of Theorem 1, we substitute $\mathfrak{p} := \binom{\boldsymbol{S}}{\boldsymbol{v}} := \binom{\mathsf{C}\boldsymbol{E}}{\boldsymbol{v}}$ for the elastic-acoustic case and $\mathfrak{p} = \mathfrak{q}$ for the electromagnetic case to obtain

$$\sum_e \frac{d}{dt} \mathcal{E}^e_d = \sum_e - \int_{\partial \hat{\mathsf{D}},N_e} \tilde{\boldsymbol{n}} \cdot \left[\left(\tilde{\mathfrak{F}} \mathfrak{q}^e \right)^* - \frac{1}{2} \left(\tilde{\mathfrak{F}} \mathfrak{q}^e \right) \right] \cdot \mathfrak{p}^e \, d\boldsymbol{s} + \int_{\hat{\mathsf{D}},N_e} J^e \mathfrak{g}^e \cdot \mathfrak{p}^e \, d\boldsymbol{r}. \tag{6.2}$$

We divide the surface integrals into two groups, namely, surface integrals associated with conforming and with nonconforming interfaces. The former group has been shown to be nonpositive as in the proof of Theorem 1. We therefore need to consider only the latter group, for which we take a typical nonconforming interface and its contributing surface integrals as in section 5. We shall show that the nonconforming contribution is also nonpositive.

The surface integral contributed from element e_0, with the contravariant fluxes projected from mortars, can be written as

$$
\begin{aligned}
&-\int_{f_{e_0},N^{e_0}} \left[\tilde{\tilde{\mathfrak{F}}}^*_{e_0} - \frac{1}{2}\tilde{\tilde{\mathfrak{F}}}^-_{e_0}\right]\cdot \mathfrak{p}^{e_0}\, d\boldsymbol{r} \\
&\overset{\text{using quadrature}}{=} -\left(\mathbf{p}^{e_0}\right)^T \mathbf{M}^{e_0}\left[\tilde{\mathbf{F}}^*_{e_0} - \frac{1}{2}\tilde{\mathbf{F}}^-_{e_0}\right] \\
&\overset{\text{using (5.6) and (5.8)}}{=} -\sum_{i=1}^{N_a}\left(\mathbf{p}^{e_0}\right)^T \mathscr{R}^{m_i\to e_0}\left[\tilde{\mathbf{F}}^*_{m_i} - \frac{1}{2}\tilde{\mathbf{F}}^-_{m_i}\right] \\
&\overset{\text{using (5.3) and (5.7)}}{=} -\sum_{i=1}^{N_a}\left(\mathbf{p}^{m_i^-}\right)^T \mathscr{M}^{m_i}\left[\tilde{\mathbf{F}}^*_{m_i} - \frac{1}{2}\tilde{\mathbf{F}}^-_{m_i}\right] \\
&\overset{\text{using quadrature}}{=} -\sum_{i=1}^{N_a}\int_{\mathcal{M}_i,N_{m_i}} \left[\tilde{\tilde{\mathfrak{F}}}^*_{m_i} - \frac{1}{2}\tilde{\tilde{\mathfrak{F}}}^-_{m_i}\right]\cdot \mathfrak{p}^{m_i^-}\, d\boldsymbol{s} \\
&\overset{\text{by definition}}{=} -\sum_{i=1}^{N_a}\int_{\mathcal{M}_i,N_{m_i}} \tilde{\boldsymbol{n}}\cdot\left[\left(\tilde{\tilde{\mathfrak{F}}}\left(\mathfrak{q}^{m_i}\right)\right)^* - \frac{1}{2}\tilde{\tilde{\mathfrak{F}}}\left(\mathfrak{q}^{m_i^-}\right)\right]\cdot \mathfrak{p}^{m_i^-}\, d\boldsymbol{s}.
\end{aligned}
$$

For each contributing element e_i, $i = 1,\dots,N_a$, the surface integral on face f_{e_i}, with the contravariant fluxes projected from mortars, is

$$
\begin{aligned}
&-\int_{f_{e_i},N^{e_i}} \left[\tilde{\tilde{\mathfrak{F}}}^*_{e_i} - \frac{1}{2}\tilde{\tilde{\mathfrak{F}}}^-_{e_i}\right]\cdot \mathfrak{p}^{e_i}\, d\boldsymbol{r} \\
&\overset{\text{using quadrature}}{=} -\left(\mathbf{p}^{e_i}\right)^T \mathbf{M}^{e_i}\left[\tilde{\mathbf{F}}^*_{e_i} - \frac{1}{2}\tilde{\mathbf{F}}^-_{e_i}\right] \\
&\overset{\text{using (5.10) and (5.12)}}{=} -\left(\mathbf{p}^{e_i}\right)^T \mathscr{R}^{m_i\to e_i}\left[\tilde{\mathbf{F}}^*_{m_i} - \frac{1}{2}\tilde{\mathbf{F}}^+_{m_i}\right] \\
&\overset{\text{using (5.4) and (5.11)}}{=} -\left(\mathbf{p}^{m_i^+}\right)^T \mathscr{M}^{m_i}\left[\tilde{\mathbf{F}}^*_{m_i} - \frac{1}{2}\tilde{\mathbf{F}}^+_{m_i}\right] \\
&\overset{\text{using quadrature}}{=} -\int_{\mathcal{M}_i,N_{m_i}} \left[\tilde{\tilde{\mathfrak{F}}}^*_{m_i} - \frac{1}{2}\tilde{\tilde{\mathfrak{F}}}^+_{m_i}\right]\cdot \mathfrak{p}^{m_i^+}\, d\boldsymbol{s} \\
&\overset{\text{by definition}}{=} -\int_{\mathcal{M}_i,N_{m_i}} \tilde{\boldsymbol{n}}\cdot\left[\left(\tilde{\tilde{\mathfrak{F}}}\left(\mathfrak{q}^{m_i}\right)\right)^* - \frac{1}{2}\tilde{\tilde{\mathfrak{F}}}\left(\mathfrak{q}^{m_i^+}\right)\right]\cdot \mathfrak{p}^{m_i^+}\, d\boldsymbol{s}.
\end{aligned}
$$

Therefore, we have shown that each nonconforming interface consisting of faces f_{e_i} of contributing elements e_i, $i = 0,\dots,N_a$, is equivalent to $2N_a$ conforming faces associated with N_a mortars $\mathcal{M}_j$, $j = 1,\dots,N_a$. That is, the surface integrals in (6.2) in fact consist of conforming interfaces—either the original conforming interfaces or equivalent conforming mortars. The stability proof of Theorem 1 for conforming faces can now be applied to complete the proof. ∎

When the strong outflow condition is not satisfied, i.e., when LGL quadrature is used as in Proposition 1, we have the following stability.

THEOREM 3 (stability for nonconforming meshes with LGL quadratures). *Suppose all assumptions in Theorem 2 hold except that the LGL quadrature is employed. Then the DGSEM discretization is stable in the sense that*

$$
\frac{d}{dt}\mathcal{E}_d \le \frac{1}{2}\left((1+2c)\,\mathcal{E}_d + \|\Pi\mathfrak{g}\|^2_{\mathcal{D}^{n_{el}},d}\right),
$$

where the small constant c converges to zero if the exact solution $\mathfrak{q}$ is sufficiently smooth.

Proof. When the numerical integration is not exact, we have the extra term

$$\sum_e \int_{\partial\hat{\mathsf{D}},N_e} \tilde{\boldsymbol{n}} \cdot \left[\tilde{\mathfrak{F}}\mathfrak{q}^e \Big|_{\partial\hat{\mathsf{D}}} - \tilde{\mathfrak{F}}\mathfrak{q}^e \right] \cdot \mathfrak{p}^e \, d\boldsymbol{s}, \tag{6.3}$$

which can be shown to be small as

$$\sum_e \int_{\partial\hat{\mathsf{D}},N_e} \tilde{\boldsymbol{n}} \cdot \left[\tilde{\mathfrak{F}}\mathfrak{q}^e \Big|_{\partial\hat{\mathsf{D}}} - \tilde{\mathfrak{F}}\mathfrak{q}^e \right] \cdot \mathfrak{p}^e \, d\boldsymbol{s} \le c\mathcal{E}_d. \tag{6.4}$$

We now provide an explicit estimate for the constant c to show that c is indeed negligible. It is sufficient to estimate the error for contributing element e_i whose face f_{e_i} is on the "+" side of a mortar. From the weak outflow identity (5.15) and the triangle inequality, we have

$$\begin{aligned}
&\left| \int_{e_i,N_{e_i}} \tilde{\boldsymbol{n}} \cdot \left[\tilde{\mathfrak{F}}\mathfrak{q}^{e_i} \Big|_{\partial\hat{\mathsf{D}}} - \tilde{\mathfrak{F}}\mathfrak{q}^{e_i} \right] \cdot \mathfrak{p}^{e_i} \, d\boldsymbol{s} \right| \\
&\quad \le \left| \int_{\mathcal{M}_i,N_{m_i}} \tilde{\boldsymbol{n}} \cdot \tilde{\mathfrak{F}}\mathfrak{q}^{e_i} \Big|_{\partial\hat{\mathsf{D}}} \cdot \mathfrak{p}^{e_i} \, d\boldsymbol{s} - \int_{\mathcal{M}_i} \tilde{\boldsymbol{n}} \cdot \tilde{\mathfrak{F}}\mathfrak{q}^{e_i} \Big|_{\partial\hat{\mathsf{D}}} \cdot \mathfrak{p}^{e_i} \, d\boldsymbol{s} \right| \\
&\qquad + \left| \int_{\mathcal{M}_i,N_{e_i}} \tilde{\boldsymbol{n}} \cdot \tilde{\mathfrak{F}}\mathfrak{q}^{e_i} \Big|_{\partial\hat{\mathsf{D}}} \cdot \mathfrak{p}^{e_i} \, d\boldsymbol{s} - \int_{\mathcal{M}_i} \tilde{\boldsymbol{n}} \cdot \tilde{\mathfrak{F}}\mathfrak{q}^{e_i} \Big|_{\partial\hat{\mathsf{D}}} \cdot \mathfrak{p}^{e_i} \, d\boldsymbol{s} \right|.
\end{aligned}$$

Note that both terms on the right-hamd side of the preceding inequality are of the same type, namely, the error between LGL quadrature integration and exact integration for polynomial of order $2N_{e_i}$. Since $N_{m_i} \ge N_{e_i}$, we need to estimate only the second term. Using an error estimate from [1] together with Stirling's formula, we have

$$\begin{aligned}
&\left| \int_{\mathcal{M}_i,N_{e_i}} \tilde{\boldsymbol{n}} \cdot \tilde{\mathfrak{F}}\mathfrak{q}^{e_i} \Big|_{\partial\hat{\mathsf{D}}} \cdot \mathfrak{p}^{e_i} \, d\boldsymbol{s} - \int_{\mathcal{M}_i} \tilde{\boldsymbol{n}} \cdot \tilde{\mathfrak{F}}\mathfrak{q}^{e_i} \Big|_{\partial\hat{\mathsf{D}}} \cdot \mathfrak{p}^{e_i} \, d\boldsymbol{s} \right| \\
&\quad = \mathcal{O}\left(\frac{N_{e_i}+1}{2N_{e_i}+1} \left(\frac{N_{e_i}-1}{N_{e_i}} \right)^{4N_{e_i}-2} \frac{1}{2^{2N_{e_i}}} h_e^{2N_{e_i}} \right),
\end{aligned}$$

which shows that the error introduced by having the weak outflow condition (instead of the strong one for which the additional error (6.3) is zero) is decaying exponentially with respect to the solution order N_{e_i}, and at the rate $2N_{e_i}$, i.e., $h_e^{2N_{e_i}}$, with respect to h_e. Compared to the optimal error rate with respect to h_e and N_{e_i} in (7.1)–(7.2), the error rate resulting from the weak outflow condition is much smaller. ∎

Remark 2. By virtue of both h and p estimates above, we see that even though the inexactness of the LGL quadrature violates the strong outflow condition and hence generates additional boundary terms when integration by parts is performed, these

terms are negligible. From now on, if LGL quadrature is used, we implicitly absorb the additional error terms arising from the weak outflow condition into constant in the convergence estimate, as in Theorem 4, or we simply ignore them.

7. Convergence rate analysis. The previous sections show that our discrete approximations, both conforming and nonconforming, are stable. Together with consistency, to be shown below, our approximations are convergent by the Lax–Ritchmyer equivalence theorem. The direct consequence is that the solution can grow at most exponentially in time, which is typical for Lax–Ritchmyer type of convergence. This kind of convergence result is interesting for theoretical analysis, but may not be appropriate for assessing the actual convergence rate of a numerical method. Fortunately, Hesthaven and Warburton [13] show that a direct convergence analysis is possible, allowing a much better upper bound on the error estimate. We adapt this type of direct convergence analysis to derive a priori error bounds for our nonconforming approximations.

Recall that interpolation introduces truncation and aliasing errors [8, 18], and hence interpolation is generally different from projection, which has only truncation error. For sufficiently smooth functions, however, the aliasing error either is spectrally small [8, 12, 18] or can be made equal to zero [13]. Following [13], we shall make no distinction between interpolation and projection in what remains.

The following conventions are used in this section. We reserve $\mathfrak{q}$ for the unknown exact solution, $\mathcal{I}_{N_e}\mathfrak{q}$ for the projection of $\mathfrak{q}$ onto $\mathcal{P}_{N_e}$, and $\mathfrak{q}_{N_e}$ for the solution of the discrete form (3.2) restricted on element e. In addition, C denotes a generic constant that may have different values in different contexts, $\mathfrak{q}_d$ is defined by $\mathfrak{q}_d|_{\mathsf{D}^e} = \mathfrak{q}_{N_e}$, and finally a dummy variable q lives in different spaces for different inequalities. To begin, we recall the following fundamental *hp* approximation error bounds [2, 3, 4]:

$$\|q - \mathcal{I}_{N_e} q\|_{H^r(\mathsf{D}^e)} \leq C \frac{h_e^{\sigma_e - r}}{N_e^{s_e - r}} \|q\|_{H^{s_e}(\mathsf{D}^e)}, \quad 0 \leq r \leq s_e, \tag{7.1}$$

$$\|q - \mathcal{I}_{N_e} q\|_{\partial\mathsf{D}^e} \leq C \frac{h_e^{\sigma_e - 1/2}}{N_e^{s_e - 1/2}} \|q\|_{H^{s_e}(\mathsf{D}^e)}, \quad s_e > \frac{1}{2}, \tag{7.2}$$

with $h_e = diam\,(\mathsf{D}^e)$, $\sigma_e = \min\{N_e + 1, s_e\}$, and $\|\cdot\|_{H^r(\mathsf{D}^e)}$ denoting the usual Sobolev norm.

For approximation using tensor product LGL quadrature, the following equivalence of the discrete and continuous norm, an extension of the one-dimensional version in [12], is useful in passing from the discrete norm to the continuous one and vice versa: for all $q \in \mathcal{P}_N$,

$$\|q\|_{\hat{\mathsf{D}}} \leq \|q\|_{\hat{\mathsf{D}},N} \leq \left(2 + \frac{1}{N}\right)^{3/2} \|q\|_{\hat{\mathsf{D}}} \text{ and } \|q\|_{\partial\hat{\mathsf{D}}} \leq \|q\|_{\partial\hat{\mathsf{D}},N} \leq \left(2 + \frac{1}{N}\right) \|q\|_{\partial\hat{\mathsf{D}}}.$$

We first derive the convergence rate for conforming meshes. Since the electromagnetic, acoustic, elastic, and coupled acoustic-elastic wave equations are similar, we analyze the electromagnetic case and leave out details of the others. Denote $T^{\mathfrak{q}} = [T^{\boldsymbol{E}}, T^{\boldsymbol{H}}]^T$ as the truncation error that results from substituting the exact solution $\mathfrak{q}$ in the discrete equation (3.2). Using the fact that $\mathfrak{q}$ satisfies the Maxwell's

equations, we have

$$\begin{aligned}
&\left(\boldsymbol{\ell}_k, \mathcal{I}_{N_e} T^{\boldsymbol{E}}\right)_{\mathsf{D}^e, N_e} \\
&\quad = \left(\boldsymbol{\ell}_k, \mathcal{I}_{N_e} \nabla \times (\boldsymbol{H} - \mathcal{I}_{N_e} \boldsymbol{H})\right)_{\mathsf{D}^e, N_e} \\
&\qquad + \left(\boldsymbol{\ell}_k, \frac{1}{2\,\{\{Z\}\}} \boldsymbol{n} \times \left(Z^+ \left[\mathcal{I}_{N_e} \boldsymbol{H}\right] - \boldsymbol{n} \times \left[\mathcal{I}_{N_e} \boldsymbol{E}\right]\right)\right)_{\partial \mathsf{D}^e, N_e} \qquad \forall \boldsymbol{\ell}_k \in \mathcal{P}_{N_e} \\
&\left(\boldsymbol{\ell}_k, \mathcal{I}_{N_e} T^{\boldsymbol{H}}\right)_{\mathsf{D}^e, N_e} \\
&\quad = \left(\boldsymbol{\ell}_k, \mathcal{I}_{N_e} \nabla \times (\boldsymbol{E} - \mathcal{I}_{N_e} \boldsymbol{E})\right)_{\mathsf{D}^e, N_e} \\
&\qquad + \left(\boldsymbol{\ell}_k, \frac{1}{2\,\{\{Y\}\}} \boldsymbol{n} \times \left(Y^+ \left[\mathcal{I}_{N_e} \boldsymbol{E}\right] + \boldsymbol{n} \times \left[\mathcal{I}_{N_e} \boldsymbol{H}\right]\right)\right)_{\partial \mathsf{D}^e, N_e} \qquad \forall \boldsymbol{\ell}_k \in \mathcal{P}_{N_e},
\end{aligned}$$

where, through the end of this section, μ and ε are assumed to be elementwise constant, and the mesh is affine. Note that since the truncation errors for the electric and magnetic equations are similar, we need to estimate only the former and infer the latter. Since $\mathcal{I}_{N_e} T^{\boldsymbol{E}} \in \mathcal{P}_{N_e}$, we can take $\boldsymbol{\ell}_k = \mathcal{I}_{N_e} T^{\boldsymbol{E}}$ and use the Cauchy–Schwarz inequality together with the equivalence of discrete and continuous norms to obtain

$$\begin{aligned}
\left\|\mathcal{I}_{N_e} T^{\boldsymbol{E}}\right\|^2_{\mathsf{D}^e, N_e} \leq\ & 27^2 \left\|\mathcal{I}_{N_e} \nabla \times (\boldsymbol{H} - \mathcal{I}_{N_e} \boldsymbol{H})\right\|_{\mathsf{D}^e} \left\|\mathcal{I}_{N_e} T^{\boldsymbol{E}}\right\|_{\mathsf{D}^e} \\
&+ 9^2 \left\|\frac{1}{2\,\{\{Z\}\}} \boldsymbol{n} \times \left(Z^+ \left[\mathcal{I}_{N_e} \boldsymbol{H}\right] - \boldsymbol{n} \times \left[\mathcal{I}_{N_e} \boldsymbol{E}\right]\right)\right\|_{\partial \mathsf{D}^e} \left\|\mathcal{I}_{N_e} T^{\boldsymbol{E}}\right\|_{\partial \mathsf{D}^e}.
\end{aligned}$$

Now using the following inverse trace inequality [25] for all $q \in \mathcal{P}_{N_e}$,

$$\|q\|_{\partial \mathsf{D}^e} \leq C \frac{N_e}{h_e^{1/2}} \|q\|_{\mathsf{D}^e} \tag{7.3}$$

yields

$$\begin{aligned}
\left\|\mathcal{I}_{N_e} T^{\boldsymbol{E}}\right\|_{\mathsf{D}^e, N_e} \leq\ & C \left\|\mathcal{I}_{N_e} \nabla \times (\boldsymbol{H} - \mathcal{I}_{N_e} \boldsymbol{H})\right\|_{\mathsf{D}^e} \\
&+ C \frac{N_e}{h_e^{1/2}} \left\|\frac{1}{2\,\{\{Z\}\}} \left(Z^+ \left[\mathcal{I}_{N_e} \boldsymbol{H}_\tau\right] - \left[\mathcal{I}_{N_e} \boldsymbol{E}_\tau\right]\right)\right\|_{\partial \mathsf{D}^e},
\end{aligned} \tag{7.4}$$

where we have introduced the tangent components of $\boldsymbol{E}$ and $\boldsymbol{H}$ as

$$\boldsymbol{E}_\tau = \boldsymbol{n} \times (\boldsymbol{n} \times \boldsymbol{E}), \quad \boldsymbol{H}_\tau = \boldsymbol{n} \times \boldsymbol{H}.$$

We now have the following consistency result.

LEMMA 1 (consistency). *Suppose that each component* $\mathfrak{q}_i^e \in H^{s_e}(\mathsf{D}^e), s_e \geq 3/2$, *for* $i = 1, \ldots, d$, *with* $d = 6$ *for the electromagnetic case and* $d = 12$ *for the elastic-acoustic case. Furthermore, assume that* μ *and* ε (λ *and* μ *for the elastic-acoustic case) are elementwise constant, the mesh is affine, and the hp-nonconforming approximation in section* 5 *is used. There exists a constant* C *dependent on* s, *angle condition of* D^e, *and local values of* μ *and* ε (λ *and* μ *for elastic-acoustic case) but independent of* $\mathfrak{q}, h_e$, *and* N_e *such that*

$$\left\|\mathcal{I}_{N_e} T^{\mathfrak{q}}\right\|_{\mathcal{D}^{n_{el},d}} \leq C \sum_e \frac{h_e^{\sigma_e - 1}}{N_e^{s_e - 3/2}} \|\mathfrak{q}\|_{[H^{s_e}(\mathsf{D}^e)]^d}.$$

Proof. Since the proofs for the electromagnetic and elastic-acoustic cases are similar, we provide only the proof for the former. We begin by estimating the bound for the first term on the right-hand side of (7.4). Using approximation result (7.1) we have

$$\|\mathcal{I}_{N_e}\nabla\times(\boldsymbol{H}-\mathcal{I}_{N_e}\boldsymbol{H})\|_{\mathsf{D}^e}\leq\|\nabla\times(\boldsymbol{H}-\mathcal{I}_{N_e}\boldsymbol{H})\|_{\mathsf{D}^e}\leq C\frac{h_e^{\sigma_e-1}}{N_e^{s_e-1}}\|\boldsymbol{H}\|_{[H^{s_e}(\mathsf{D}^e)]^3}.$$

To estimate the second term we use the regularity of the exact solution, i.e., the tangent component of the field is continuous, and the triangle inequality to bound $\|[\mathcal{I}_{N_e}\boldsymbol{H}_\tau]\|_{\partial\mathsf{D}^e}$, and hence similarly for $\|[\mathcal{I}_{N_e}\boldsymbol{E}_\tau]\|_{\partial\mathsf{D}^e}$, as

$$\|[\mathcal{I}_{N_e}\boldsymbol{H}_\tau]\|_{\partial\mathsf{D}^e}\leq\left\|\boldsymbol{H}_\tau^- -\mathcal{I}_{N_e}\boldsymbol{H}_\tau^-\right\|_{\partial\mathsf{D}^e}+\left\|\boldsymbol{H}_\tau^+-\mathcal{I}_{N_e}\boldsymbol{H}_\tau^+\right\|_{\partial\mathsf{D}^e}.$$

Two terms on the right-hand side of the preceding inequality are of the same type, and therefore we need to estimate only the bound for the first term. But this is straightforward using (7.2), i.e.,

$$\left\|\boldsymbol{H}_\tau^- -\mathcal{I}_{N_e}\boldsymbol{H}_\tau^-\right\|_{\partial\mathsf{D}^e}\leq C\frac{h_e^{\sigma_e-1/2}}{N_e^{s_e-1/2}}\|\boldsymbol{H}_\tau\|_{[H^{s_e}(\mathsf{D}^e)]^3}\leq C\frac{h_e^{\sigma_e-1/2}}{N_e^{s_e-1/2}}\|\boldsymbol{H}\|_{[H^{s_e}(\mathsf{D}^e)]^3}.$$

Now combining the above estimates for both terms on the right-hand side of (7.4), summing over all elements, and using the discrete Hölder's inequality completes the proof. ∎

Remark 3. Note that the proof of Lemma 1 is carried out for conforming meshes. However, by the proof of Theorem 2, the surface integrals in (6.2) in fact consist of conforming interfaces—either the original conforming interfaces or equivalent conforming mortars. Hence, the proof for nonconforming meshes is almost identical except for bounding the boundary terms which are now defined on the mortars instead of on the contributing element faces. But the fields on the mortars are the L^2 orthogonal projections of those on the contributing element faces, which implies that L^2 norms of fields on mortars are at most those on contributing element faces. This shows that the proof for conforming meshes is sufficient. In the rest of the paper, analyses are therefore carried out for the conforming approximation.

We now state the first convergence result.

THEOREM 4. *Assume* $\mathfrak{q}^e\in[H^{s_e}(\mathsf{D}^e)]^d, s_e\geq 3/2$, *with* $d=6$ *for the electromagnetic case and* $d=12$ *for the elastic-acoustic case. In addition, suppose* $\mathfrak{q}_d(0)=\Pi\mathfrak{q}(0)$. *Furthermore, assume that* μ *and* ε (λ *and* μ *for the elastic-acoustic case) are elementwise constant, the mesh is affine, and the hp-nonconforming approximation in section* 5 *is used. Then, the solution* $\mathfrak{q}_d$ *of the discrete form* (3.2) *converges to the exact solution* $\mathfrak{q}$*; i.e., there exists a constant* C *that depends only on the angle condition of* D^e, s, *and the material constants* μ *and* ε (λ *and* μ *for the elastic-acoustic case) such that*

$$\|\mathfrak{q}(t)-\mathfrak{q}_d(t)\|_{\mathcal{D}^{n_{el},d}}\leq C\sum_e\left[\frac{h_e^{\sigma_e}}{N_e^{s_e}}\|\mathfrak{q}(t)\|_{[H^{s_e}(\mathsf{D}^e)]^d}+t\frac{h_e^{\sigma_e-1}}{N_e^{s_e-3/2}}\max_{[0,t]}\|\mathfrak{q}(t)\|_{[H^{s_e}(\mathsf{D}^e)]^d}\right].$$

Proof. We begin the proof with the following identities:

$$
\begin{aligned}
&\left(\mathcal{I}_{N_e}\boldsymbol{E}-\boldsymbol{E}_d^e,\mathcal{I}_{N_e}T^{\boldsymbol{E}}\right)_{\mathsf{D}^e,N_e}\\
&\quad=\left(\mathcal{I}_{N_e}\boldsymbol{E}-\boldsymbol{E}_d^e,\varepsilon\frac{\partial\left(\mathcal{I}_{N_e}\boldsymbol{E}-\boldsymbol{E}_d^e\right)}{\partial t}\right)_{\mathsf{D}^e,N_e}\\
&\qquad-\left(\mathcal{I}_{N_e}\boldsymbol{E}-\boldsymbol{E}_d^e,\mathcal{I}_{N_e}\nabla\times\left(\mathcal{I}_{N_e}\boldsymbol{H}-\boldsymbol{H}_d^e\right)\right)_{\mathsf{D}^e,N_e}\\
&\qquad+\left(\mathcal{I}_{N_e}\boldsymbol{E}-\boldsymbol{E}_d^e,\frac{1}{2\left\{\{Z\}\right\}}\boldsymbol{n}\times\left(Z^+\left[\mathcal{I}_{N_e}\boldsymbol{H}-\boldsymbol{H}_d^e\right]-\boldsymbol{n}\times\left[\mathcal{I}_{N_e}\boldsymbol{E}-\boldsymbol{E}_d^e\right]\right)\right)_{\partial\mathsf{D}^e,N_e},\\
&\qquad\left(\mathcal{I}_{N_e}\boldsymbol{H}-\boldsymbol{H}_d^e,\mathcal{I}_{N_e}T^{\boldsymbol{H}}\right)_{\mathsf{D}^e,N_e}\\
&\quad=\left(\mathcal{I}_{N_e}\boldsymbol{H}-\boldsymbol{H}_d^e,\mu\frac{\partial\left(\mathcal{I}_{N_e}\boldsymbol{H}-\boldsymbol{H}_d^e\right)}{\partial t}\right)_{\mathsf{D}^e,N_e}\\
&\qquad+\left(\mathcal{I}_{N_e}\boldsymbol{H}-\boldsymbol{H}_d^e,\mathcal{I}_{N_e}\nabla\times\left(\mathcal{I}_{N_e}\boldsymbol{E}-\boldsymbol{E}_d^e\right)\right)_{\mathsf{D}^e,N_e}\\
&\qquad-\left(\mathcal{I}_{N_e}\boldsymbol{H}-\boldsymbol{H}_d^e,\frac{1}{2\left\{\{Y\}\right\}}\boldsymbol{n}\times\left(Y^+\left[\mathcal{I}_{N_e}\boldsymbol{E}-\boldsymbol{E}_d^e\right]+\boldsymbol{n}\times\left[\mathcal{I}_{N_e}\boldsymbol{H}-\boldsymbol{H}_d^e\right]\right)\right)_{\partial\mathsf{D}^e,N_e},
\end{aligned}
$$

where we have substituted the exact solution into the discrete equation (3.2) and used $\mathcal{I}_{N_e}\boldsymbol{E}-\boldsymbol{E}_d^e$ and $\mathcal{I}_{N_e}\boldsymbol{H}-\boldsymbol{H}_d^e$ as test functions for the electric and magnetic equations, respectively.

Following the proof of Theorem 2, we integrate the preceding equations by parts, sum up the resulting equations, cancel the volume terms involving the fluxes, and use the nonpositiveness of the boundary integrals to arrive at

$$
\frac{d}{dt}\left\|\Pi\mathfrak{q}-\mathfrak{q}_d\right\|_{\mathcal{D}^{n_{\mathrm{el}}},d}^2\le C\sum_e\left(\mathcal{I}_{N_e}\mathfrak{q}-\mathfrak{q}_d^e,\mathcal{I}_{N_e}T^{\mathfrak{q}}\right)_{\mathsf{D}^e,N_e},
$$

where we have used the fact that the material constants μ and ε are bounded away from zero. Next, we use Cauchy–Schwarz and then the discrete Hölder's inequalities, and then apply the consistency result of Lemma 1 to obtain

$$
\frac{d}{dt}\left\|\Pi\mathfrak{q}-\mathfrak{q}_d\right\|_{\mathcal{D}^{n_{\mathrm{el}}},d}\le C\sum_e\frac{h_e^{\sigma_e-1}}{N_e^{s_e-3/2}}\left\|\mathfrak{q}\right\|_{[H^{s_e}(\mathsf{D}^e)]^d}\le C\sum_e\frac{h_e^{\sigma_e-1}}{N_e^{s_e-3/2}}\max_{[0,t]}\left\|\mathfrak{q}\right\|_{[H^{s_e}(\mathsf{D}^e)]^d},
$$

which, after integrating in time, yields

$$
\left\|\Pi\mathfrak{q}\left(t\right)-\mathfrak{q}_d\left(t\right)\right\|_{\mathcal{D}^{n_{\mathrm{el}}},d}\le Ct\sum_e\frac{h_e^{\sigma_e-1}}{N_e^{s_e-3/2}}\max_{[0,t]}\left\|\mathfrak{q}\left(t\right)\right\|_{[H^{s_e}(\mathsf{D}^e)]^d},
$$

where we have used $\mathfrak{q}_d(0)=\Pi\mathfrak{q}(0)$. Now, using the triangle inequality, we have

$$
\left\|\mathfrak{q}\left(t\right)-\mathfrak{q}_d\left(t\right)\right\|_{\mathcal{D}^{n_{\mathrm{el}}},d}\le\left\|\mathfrak{q}\left(t\right)-\Pi\mathfrak{q}\left(t\right)\right\|_{\mathcal{D}^{n_{\mathrm{el}}},d}+\left\|\Pi\mathfrak{q}\left(t\right)-\mathfrak{q}_d\left(t\right)\right\|_{\mathcal{D}^{n_{\mathrm{el}}},d}.
$$

Finally, using the equivalence of the discrete and continuous norms and (7.1) ends the proof. ∎

Remark 4. Since all norms are equivalent in finite dimensional spaces, the result of Theorem 4 holds for other norms as well, with possibly different constant C. In particular, we have

$$
\begin{aligned}
&\sum_e\left\|\mathfrak{q}\left(t\right)-\mathfrak{q}_d\left(t\right)\right\|_{\mathsf{D}^e,N_e}\\
&\qquad\le C\sum_e\left[\frac{h_e^{\sigma_e}}{N_e^{s_e}}\left\|\mathfrak{q}\left(t\right)\right\|_{[H^{s_e}(\mathsf{D}^e)]^d}+t\frac{h_e^{\sigma_e-1}}{N_e^{s_e-3/2}}\max_{[0,t]}\left\|\mathfrak{q}\left(t\right)\right\|_{[H^{s_e}(\mathsf{D}^e)]^d}\right].
\end{aligned}
$$

Remark 5. We again emphasize that the LGL quadrature introduces additional error terms when the discrete integration by parts is performed. However, they are shown to be negligible in Theorem 3 and Remark 2, so their absence in the proof of Theorem 4 is justified. The proof for the LG quadrature follows exactly the same lines and hence is omitted here. The only difference is that all the numerical integrations are exact, and therefore there is no need to invoke the equivalence of discrete and continuous norms.

The proof of Theorem 4 is simple since it directly uses the consistency and stability results. Nevertheless, the rate is suboptimal in h by a factor of $1/2$ and in N by 1 compared to the DG literature. This loss is incurred when estimating the truncation error and using the inverse trace inequality (7.3). This begs for a more sophisticated proof that does not lead to a deterioration of the optimal convergence rate. Inspired by the work of Warburton [28], we present a proof that improves the convergence rate in h by a factor of $1/2$ and in N by 1. We start by rewriting (3.2), after integrating by parts, for an affine mesh and elementwise constant materials, as

$$\begin{aligned}&\sum_e \int_{\mathsf{D}^e} \frac{\partial \mathfrak{q}_d^e}{\partial t}\cdot \mathfrak{p}^e\, d\boldsymbol{x} - \int_{\mathsf{D}^e} \mathfrak{F}\mathfrak{q}_d^e \cdot (\nabla_{\boldsymbol{x}}\cdot \mathfrak{p}^e)\, d\boldsymbol{x}\\ &\quad + \int_{\partial \mathsf{D}^e} \tilde{\boldsymbol{n}}\cdot \left[(\mathfrak{F}\mathfrak{q}_d^e)^*\right]\cdot \mathfrak{p}^e\, d\boldsymbol{s} = \sum_e \int_{\mathsf{D}^e} \mathfrak{g}^e\cdot \mathfrak{p}^e\, d\boldsymbol{x} + \mathcal{R}_e \quad \forall \mathfrak{p}\in \mathcal{V}_d,\end{aligned} \tag{7.5}$$

where, by the proof of Theorem 3, $\mathcal{R}_e = o(\frac{h_e^{\sigma_e}}{N_e^{s_e}})$ and $\mathcal{R}_e = 0$ for LGL and LG quadratures, respectively. Since the exact solution $\mathfrak{q}$ also satisfies (7.5) with $\mathcal{R}_e = 0$, we obtain

$$\begin{aligned}&\sum_e \int_{\mathsf{D}^e} \frac{\partial\left(\mathfrak{q}-\mathfrak{q}_d^e\right)}{\partial t}\cdot \mathfrak{p}^e\, d\boldsymbol{x} - \int_{\mathsf{D}^e} \mathfrak{F}\left(\mathfrak{q}-\mathfrak{q}_d^e\right)\cdot (\nabla_{\boldsymbol{x}}\cdot \mathfrak{p}^e)\, d\boldsymbol{x}\\ &\quad + \int_{\partial \mathsf{D}^e} \tilde{\boldsymbol{n}}\cdot \left(\mathfrak{F}\left(\mathfrak{q}-\mathfrak{q}_d^e\right)\right)^*\cdot \mathfrak{p}^e\, d\boldsymbol{s} = -\sum_e \mathcal{R}_e \quad \forall \mathfrak{p}\in \mathcal{V}_d.\end{aligned} \tag{7.6}$$

Next, adding and subtracting the elemental projection of the exact solution, i.e., $\mathcal{I}_{N_e}\mathfrak{q}$, yields

$$\begin{aligned}&\sum_e \int_{\mathsf{D}^e} \frac{\partial\left(\mathcal{I}_{N_e}\mathfrak{q}-\mathfrak{q}_d^e\right)}{\partial t}\cdot \mathfrak{p}^e\, d\boldsymbol{x} - \int_{\mathsf{D}^e} \mathfrak{F}\left(\mathcal{I}_{N_e}\mathfrak{q}-\mathfrak{q}_d^e\right)\cdot (\nabla_{\boldsymbol{x}}\cdot \mathfrak{p}^e)\, d\boldsymbol{x}\\ &\quad + \int_{\partial \mathsf{D}^e} \tilde{\boldsymbol{n}}\cdot \left(\mathfrak{F}\left(\mathcal{I}_{N_e}\mathfrak{q}-\mathfrak{q}_d^e\right)\right)^*\cdot \mathfrak{p}^e\, d\boldsymbol{s}\\ &= -\sum_e \int_{\partial \mathsf{D}^e} \tilde{\boldsymbol{n}}\cdot \left(\mathfrak{F}\left(\mathfrak{q}-\mathcal{I}_{N_e}\mathfrak{q}\right)\right)^*\cdot \mathfrak{p}^e\, d\boldsymbol{s} - \mathcal{R}_e \quad \forall \mathfrak{p}\in \mathcal{V}_d,\end{aligned} \tag{7.7}$$

where we have used the linearity of $\mathfrak{F}$ and the orthogonal identity

$$\int_{\mathsf{D}^e} \left(\mathfrak{q}-\mathcal{I}_{N_e}\mathfrak{q}\right)\cdot \mathfrak{p}^e\, d\boldsymbol{x} = 0, \quad \mathfrak{p}^e \in L^2\left(\mathsf{D}^e\right)^d.$$

Now, integrating (7.7) by parts, testing the resulting equation and (7.7) with $\mathfrak{p}^e =$

$\mathcal{I}_{N_e}\mathfrak{q}-\mathfrak{q}_d^e$, and then adding them yields

$$\begin{aligned}&\frac{d}{dt}\left\|\Pi\mathfrak{q}-\mathfrak{q}_d\right\|^2_{\mathcal{D}^{n_{\mathrm{el}},d}}+\sum_e\frac{1}{2}\int_{\partial\mathsf{D}^e}\tilde{\boldsymbol{n}}\cdot\left(\mathfrak{F}\left(\mathfrak{q}-\mathcal{I}_{N_e}\mathfrak{q}\right)\right)^*\cdot\left[\mathcal{I}_{N_e}\mathfrak{q}-\mathfrak{q}_d^e\right]\,d\boldsymbol{s}+\mathcal{R}_e\\ &\quad=-\sum_e\underbrace{\int_{\partial\mathsf{D}^e}\tilde{\boldsymbol{n}}\cdot\left[\left(\mathfrak{F}\left(\mathcal{I}_{N_e}\mathfrak{q}-\mathfrak{q}_d^e\right)\right)^*-\frac{1}{2}\mathfrak{F}\left(\mathcal{I}_{N_e}\mathfrak{q}-\mathfrak{q}_d^e\right)\right]\cdot\left(\mathcal{I}_{N_e}\mathfrak{q}-\mathfrak{q}_d^e\right)\,d\boldsymbol{s}}_{K^e}.\end{aligned}\tag{7.8}$$

On the other hand, if ρ,λ,μ, and ε are bounded, the proof of Theorems 1 and 2 implies

$$K^e\geq\alpha^e\left\|[\mathcal{I}_{N_e}\mathfrak{q}-\mathfrak{q}_d^e]\right\|^2_{[L^2(\partial\mathsf{D}^e)]^d}\tag{7.9}$$

for some $\alpha^e>0$.

We are now in a position to prove the following convergence result.

THEOREM 5. *Assume* $\mathfrak{q}^e\in\left[H^{s_e}\left(\mathsf{D}^e\right)\right]^d, s_e\geq 3/2$, *with* $d=6$ *for the electromagnetic case and* $d=12$ *for the elastic-acoustic case. In addition, suppose* $\mathfrak{q}_d(0)=\Pi\mathfrak{q}(0)$. *Furthermore, assume that* μ *and* ε (λ *and* μ *for the elastic-acoustic case) are elementwise constant, the mesh is affine, and the hp-nonconforming approximation in section* 5 *is used. Then, the solution* $\mathfrak{q}_d$ *of the discrete form* (3.2) *converges to the exact solution* $\mathfrak{q}$*; i.e., there exists a constant* C *that depends only on the angle condition of* D^e, s, *and the material constants* μ *and* ε (λ *and* μ *for the elastic-acoustic case) such that*

$$\left\|\mathfrak{q}\left(t\right)-\mathfrak{q}_d\left(t\right)\right\|_{\mathcal{D}^{n_{el},d}}\leq C\sum_e\left[\frac{h_e^{\sigma_e}}{N_e^{s_e}}\left\|\mathfrak{q}\left(t\right)\right\|_{[H^{s_e}(\mathsf{D}^e)]^d}+t\frac{h_e^{\sigma_e-1/2}}{N_e^{s_e-1/2}}\max_{[0,t]}\left\|\mathfrak{q}\left(t\right)\right\|_{[H^{s_e}(\mathsf{D}^e)]^d}\right].$$

Proof. Using Young's inequality for some $\beta^e>0$ we have

$$\begin{aligned}&\sum_e\int_{\partial\mathsf{D}^e}\left|\tilde{\boldsymbol{n}}\cdot\left(\mathfrak{F}\left(\mathfrak{q}-\mathcal{I}_{N_e}\mathfrak{q}\right)\right)^*\cdot\left[\mathcal{I}_{N_e}\mathfrak{q}-\mathfrak{q}_d^e\right]\right|\,d\boldsymbol{s}\\ &\quad\leq\sum_e\beta^e\left\|\mathfrak{q}-\mathcal{I}_{N_e}\mathfrak{q}\right\|^2_{[L^2(\partial\mathsf{D}^e)]^d}+\sum_e\frac{1}{\beta^e}\left\|[\mathcal{I}_{N_e}\mathfrak{q}-\mathfrak{q}_d^e]\right\|^2_{[L^2(\partial\mathsf{D}^e)]^d},\end{aligned}\tag{7.10}$$

where we have used the linearity of $\mathfrak{F}^*$. Combining (7.8), (7.9), and (7.11) yields

$$\begin{aligned}&\frac{d}{dt}\left\|\Pi\mathfrak{q}-\mathfrak{q}_d\right\|^2_{\mathcal{D}^{n_{\mathrm{el}},d}}+\sum_e\left(\alpha-\frac{1}{\beta^e}\right)\left\|[\mathcal{I}_{N_e}\mathfrak{q}-\mathfrak{q}_d^e]\right\|^2_{[L^2(\partial\mathsf{D}^e)]^d}\\ &\quad\leq\sum_e\beta^e\left\|\mathfrak{q}-\mathcal{I}_{N_e}\mathfrak{q}\right\|^2_{[L^2(\partial\mathsf{D}^e)]^d}+\left|\mathcal{R}_e\right|.\end{aligned}\tag{7.11}$$

Next, taking $\beta^e\geq\frac{1}{\alpha^e}$ and using (7.2) gives

$$\frac{d}{dt}\left\|\Pi\mathfrak{q}-\mathfrak{q}_d\right\|^2_{\mathcal{D}^{n_{\mathrm{el}},d}}\leq C\sum_e\frac{h_e^{2\sigma_e-1}}{N_e^{2s_e-1}}\max_{[0,t]}\left\|\mathfrak{q}\right\|^2_{[H^{s_e}(\mathsf{D}^e)]^d}.$$

The rest of the proof follows similarly to that of Theorem 4. ∎

We have restricted ourselves to the case of affine hexahedral meshes and elementwise constant medium properties. This allows us to eliminate the volume integrals of fluxes on the right-hand side of (4.1) since differentiation and interpolation commute.

The discrete stability is then apparent due to the nonpositiveness of the surface integrals of fluxes. Most of the results still hold for meshes with $J\boldsymbol{a}^i$ = constant, for $i = 1, 2, 3$. In general, extensions of the results to general curvilinear meshes and varying material constants are not straightforward, as pointed out in [13]. For example, the stability, and hence convergence, results for both conforming and nonconforming approximations are still valid for meshes with curved elements and varying material constants, provided that the contravariant fluxes are polynomials with order at most N_e, i.e.,

$$\tilde{\mathfrak{F}}^i = J^e \boldsymbol{a}^i \cdot \mathfrak{F} \in \mathcal{P}_{N_e}, \quad i = 1, 2, 3, \tag{7.12}$$

for which we again have the commutativity of differentiation and interpolation. Together with the metric identities in [17], we again can eliminate the volume integrals after integrating by parts. However, this simple approach incurs loss in accuracy for the field $\mathfrak{q}$ since polynomial orders for approximating the field, geometry, and material constants are added up to N_e, as opposed to having polynomials of order N_e for the field alone.

It should be pointed out that the tensor product quadrature structure is used for efficiency in practice. It is also exploited for the discrete integration by parts to hold using the inexact quadrature rule, LGL. Other than that, it is not employed in our analysis. We therefore speculate that our results remain true for other types of meshes, e.g., affine tetrahedral meshes, as well, as long as the discrete integration by parts is possible and the commutativity of differentiation and interpolation is valid. The detailed work is, however, beyond the scope of this paper. For general curvilinear hexahedral/tetrahedral meshes (e.g., not satisfying (7.12)), it is not clear whether the volume integrals vanish (or become negative) or not since differentiation and interpolation generally do not commute (even overintegration is not helpful in this case).

8. Conclusions. We have presented an analysis of a nonconforming *hp* discontinuous Galerkin spectral element method of Kopriva [16] and Kopriva, Woodruff, and Hussaini [20] for time domain solution of wave propagation problems in acoustic, elastic, coupled elastic–acoustic, and electromagnetic media. We have proved consistency, stability, and convergence under certain conditions, i.e., affine meshes and elementwise constant medium properties, and speculated the results for more general meshes and material distributions. Our analytical results hold for both exact numerical integration using tensor product Legendre–Gauss quadrature and inexact numerical integration using tensor product Legendre–Gauss–Lobatto quadrature. The key ingredient of our proposed approach is the development of a discrete mortar-based approach for nonconforming approximations. With this mortar construction, we have shown that the proofs for nonconforming cases closely follow those for conforming ones, and the resulting convergence retains the same optimal rate as for standard DG methods. Numerical experiments in [29] for acoustic, elastic, and coupled acoustic-elastic wave propagation on *h*-nonconforming meshes confirm the theoretical rates presented here, and a further companion paper numerically demonstrates optimal convergence for electromagnetic wave propagation [7].

Acknowledgments. We thank Drs. Carsten Burstedde, Georg Stadler, and Lucas Wilcox for many fruitful discussions on their article [29], which stimulated the work presented here. We thank Prof. David Kopriva of Florida State University for his encouragement, without which this article would not have been possible. We also

thank Prof. Ivo Babuška for helpful discussions of his approximation results (7.1)–(7.2). Finally, we thank Prof. Tim Warburton for pointing out material in [28] that inspired us to improve the convergence rate in our proof. The authors would like to thank the anonymous referees for their critical and useful comments that significantly improved the paper.

REFERENCES

[1] M. Abramowitz and I. A. Stegun, eds., *Handbook of Mathematical Functions with Formulas, Graphs and Mathematical Tables*, Dover, New York, 1965.

[2] I. Babuška and M. Suri, *The hp-version of the finite element method with quasiuniform meshes*, M2AN Math. Model. Numer. Anal., 21 (1987), pp. 199–238.

[3] I. Babuška and M. Suri, *The optimal convergence rate of the p-version of the finite element method*, SIAM J. Numer. Anal., 24 (1987), pp. 750–776.

[4] I. Babuška and M. Suri, *The p and h-p versions of the finite element method, basic principles and properties*, SIAM Rev., 36 (1994), pp. 578–632.

[5] C. E. Baumann and J. Tinsley Oden, *A discontinuous hp finite element method for convection-diffusion problems*, Comput. Methods Appl. Mech. Engrg., 175 (1999), pp. 311–341.

[6] C. Bernardi, Y. Maday, and A. T. Patera, *A new nonconforming approach to domain decomposition: The mortar element method*, in Nonlinear Partial Differential Equations and Their Applications, H. Brezis and J. L. Lions, eds., Longman Scientific and Technical, Harlow, UK, 1994, pp. 13–51.

[7] T. Bui-Thanh, L. C. Wilcox, C. Burstedde, and O. Ghattas, *A discontinuous Galerkin method for electromagnetic wave propagation on h-non-conforming adapted meshes*, in preparation.

[8] C. Canuto, M. Y. Hussaini, A. Quarteroni, and T. A. Zang, *Spectral Methods: Fundamentals in Aingle Domains*, Sci. Comput., Springer-Verlag, Berlin, 2006.

[9] B. Cockburn, S. Hou, and C.-W. Shu, *TVD Runge–Kutta local projection discontinuous Galerkin finite element method for scalar conservation laws* IV: *The multidimensional case*, Math. Comp., 54 (1990), pp. 545–581.

[10] B. Cockburn, G. E. Karniadakis, and C.-W. Shu, eds., *Discontinuous Galerkin Methods: Theory, Computation and Applications*, Lect. Notes Comput. Sci. Eng. 11, Springer-Verlag, Berlin, Heidelberg, New York, 2000.

[11] B. Cockburn and C.-W. Shu, *The Runge–Kutta discontinuous Galerkin method for conservation laws* V: *Multidimensioal systems*, J. Comput. Phys., 141 (1998), pp. 199–224.

[12] J. S. Hesthaven, S. Gottlieb, and D. Gottlieb, *Spectral Methods for Time-Dependent Problems*, Cambridge Monogr. Appl. Comput. Math. 21, Cambridge University Press, Cambridge, UK, 2007.

[13] J. S. Hesthaven and T. Warburton, *Nodal high-order methods on unstructured grids.* I. *Time-domain solution of Maxwell's equations*, J. Comput. Phys., 181 (2002), pp. 186–221.

[14] J. S. Hesthaven and T. Warburton, *Nodal Discontinuous Galerkin Methods: Algorithms, Analysis, and Applications*, Texts Appl. Math. 54, Springer, New York, 2008.

[15] D. Kopriva, *Private communication*, 2010.

[16] D. A. Kopriva, *A conservative staggered-grid Chebyshev multidomain method for compressible flows.* II. *A semi-structured method*, J. Comput. Phys., 128 (1996), pp. 475–488.

[17] D. A. Kopriva, *Metric identities and the discontinuous spectral element method on curvilinear meshes*, J. Sci. Comput., 26 (2006), pp. 301–327.

[18] D. A. Kopriva, *Implementing Spectral Methods for Partial Differential Equations*, Springer, London, 2009.

[19] D. A. Kopriva and G. Gassner, *On the quadrature and weak form choices in collocation-type discontinuous Galerkin spectral element methods*, J. Sci. Comput., 44 (2010), pp. 136–155.

[20] D. A. Kopriva, S. L. Woodruff, and M. Y. Hussaini, *Computation of electromagnetic scattering with a non-conforming discontinuous spectral element method*, Internat. J. Numer. Methods Engrg., 53 (2002), pp. 105–122.

[21] H.-O. Kreiss and G. Scherer, *Method of lines for hyperbolic differential equations*, SIAM J. Numer. Anal., 29 (1992), pp. 640–646.

[22] P. D. Lax and R. D. Richtmyer, *Survey of the stability of linear finite difference equations*, Comm. Pure Appl. Math., 9 (1956), pp. 267–293.

[23] W. H. Reed and T. R. Hill, *Triangular Mesh Methods for the Neutron Transport Equation*, Technical report LA-UR-73-479, Los Alamos Scientific Laboratory, Los Alamos, NM, 1973.

[24] W. J. Rider and R. B. Lowrie, *The Use of Classical Lax-Friedrichs Riemann Solvers with Discontinuous Galerkin Methods*, Technical report LA-UR-01-1282, Los Alamos National Laboratory, Los Alamos, NM, 2001.

[25] C. Schwab, *p– and hp–finite Element Methods: Theory and Applications in Solid and Fluid Mechanics*, Oxford University Press, Oxford, UK, 1998.

[26] C.-H. Teng, B.-Y. Lin, H.-C. Chang, H.-C. Hsu, C.-N. Lin, and K.-A. Feng, *A Legendre pseudospectral penalty scheme for solving time-domain Maxwell's equations*, J. Sci. Comput., 36 (2008), pp. 351–390.

[27] E. F. Toro, *Riemann Solvers and Numerical Methods for Fluid Dynamics*, Springer, Berlin, 1999.

[28] T. Warburton, *Topics in Numerical Differential Equations*, CAAM 652 Lecture Notes, Rice University, Houston, TX, 2011.

[29] L. C. Wilcox, G. Stadler, C. Burstedde, and O. Ghattas, *A high-order discontinuous Galerkin method for wave propagation through coupled elastic-acoustic media*, J. Comput. Phys., 229 (2010), pp. 9373–9396.